



Article

A Robotic Deburring Methodology for Tool Path Planning and Process Parameter Control of a Five-Degree-of-Freedom Robot Manipulator

Wanjin Guo ^{1,2,*} , Ruifeng Li ², Yaguang Zhu ¹ , Tong Yang ¹, Rui Qin ¹ and Zhixin Hu ¹

¹ Key Laboratory of Road Construction Technology and Equipment of MOE, Chang'an University, Xi'an 710064, China; zhuyaguang@chd.edu.cn (Y.Z.); tsshangzao@163.com (T.Y.); qinrui@chd.edu.cn (R.Q.); hzxin@chd.edu.cn (Z.H.)

² State Key Laboratory of Robotics and System, Harbin Institute of Technology, Harbin 150001, China; lrf100@hit.edu.cn

* Correspondence: guowanjin@chd.edu.cn; Tel.: +86-29-82334865

Received: 2 April 2019; Accepted: 14 May 2019; Published: 17 May 2019



Abstract: Industrial robotics is a continuously developing domain, as industrial robots have demonstrated to possess benefits with regard to robotic automation solutions in the industrial automation field. In this article, a new robotic deburring methodology for tool path planning and process parameter control is presented for a newly developed five-degree-of-freedom hybrid robot manipulator. A hybrid robot manipulator with dexterous manipulation and two experimental platforms of robot manipulators are presented. A robotic deburring tool path planning method is proposed for the robotic deburring tool position and orientation planning and the robotic layered deburring planning. Also, a robotic deburring process parameter control method is proposed based on fuzzy control. Furthermore, a dexterous manipulation verification experiment is conducted to demonstrate the dexterous manipulation and the orientation reachability of the robot manipulator. Additionally, two robotic deburring experiments are conducted to verify the effectiveness of the two proposed methods and demonstrate the highly efficient and dexterous manipulation and deburring capacity of the robot manipulator.

Keywords: industrial robotics; robotic deburring; tool path planning; process parameter control; dexterous manipulation

1. Introduction

Industrial robotics with advanced technology for the industrial automation field has received considerable attention in recent years [1–6]. Although the development and application of industrial robots are confined—to a certain extent—to the field of advanced manufacturing due to the lack of rigidity and precision of an industrial robot compared to a numerical control machine, the industrial robot, as a common and less expensive alternative to the latter, has great advantages and potentials especially in some applications that require low cutting forces, low precision requirements, large-sized complex shaped parts and/or multi-faces machining in one setup. Therefore, industrial robots were extensively invented and introduced into factories for robotic machining and other applications such as spray automation, spot welding and materials handling. Such robotic automation freed humans from heavy and tedious labor and such industries rapidly retooled their manufacturing lines into robot-integrated systems. Consequently, industrial robots offer a real gain of flexibility, modularity, and access for machining on production lines, and are viable solutions for enhanced productivity, quality, and safety. Industrial robotics are being widely adopted in the robotic machining applications

and have become an area of significantly in-depth robotics research. More recent research on robotic machining and many diverse research domains have been investigated in recent years [7–14].

Several studies were concentrated on five-degree-of-freedom (five-DOF) hybrid robot manipulators for machining and fabrication applications. A five-DOF hybrid mechanism was developed, which included a synthesized two translational DOF and one rotational DOF (2T1R) parallel module [15]. A five-DOF hybrid mechanism which consists of a 3-DOF parallel platform and a X-Y table [16]. A parallel mechanism (3T1R) and a rotational table were integrated into a five-DOF hybrid robot manipulator [17]. A five-DOF hybrid mechanism was designed which includes a parallel manipulator (2T1R) with a rotational table [18]. A five-DOF hybrid mechanism including a 2-DOF redundant parallel manipulator was developed [19]. A five-DOF hybrid mechanism was investigated, consisting of a 3-DOF parallel manipulator with actuation redundancy and a 2-DOF worktable [20]. A five-DOF hybrid robot was introduced, which comprises of a parallel mechanism (1T2R) and two gantries [21]. Two five-DOF mechanisms were introduced, which are composed of a 3-DOF parallel mechanism connected in series with a 2-DOF wrist [22]. Some of the designs of these five-DOF hybrid robot manipulators are complex, since an application of the inferior-mobility robot manipulator demands a translatable table [15] or a rotatable one [16–18]. Also, the problem of achieving motion control is harder for a hybrid mechanism [19,20] with redundantly actuated joints than a non-redundantly actuated one. Moreover, a relatively small workspace for a robot manipulator is established to perform tasks [22].

Several research works are concentrated on the related technologies of robotic deburring. Practical mechanical deburring methods, including robotics for aluminum work parts and an overview of burr formation mechanism and morphology, were presented, and several deburring classifications were also proposed [23]. Also, a review of burr formation modeling and control, and factors governing milling burr formation were presented [24]. Robotic application of edge deburring with a controlled force progression pneumatic tool for a part of the manufacturing process of an aircraft engine detail was investigated [25]. A flexible robot-based cast iron deburring cell using a single-point laser displacement sensor was developed for small batch production of a robotized deburring task in a standard cast iron foundry scenario [26]. An adaptive robotic system using a custom-developed 3D laser-triangulation profilometer was developed for the robotic deburring of die-cast parts with position and orientation error correction [27]. Through discrete event simulation and 3D digital human modeling, a multi-purpose digital simulation approach was proposed for the sustainability enhancement of a real manufacturing cell of the aerospace industry, automated by robotic deburring [28].

The current research and applications of robotic deburring are mainly carried out by one or more traditional and commercial six-degree-of-freedom (six-DOF) serial industrial robot manipulators, which are not always suitable for the robotic deburring of complex shaped parts with highly dexterous orientations adjustment and efficient multi-faces deburring in one setup because of the defective nature of this kind of serial robot manipulator, e.g., the weakened structural rigidity of the extended robot manipulator when it is reaching far deburring position with a cantilever-beam-like structure, and the poor accessibility and small safety margins between robot manipulator and workpiece resulting from its difficulties in both obstacle avoidance adjustment and deburring orientation adjustment.

Several studies investigating tool path adaptation and process parameter control for robotic deburring were presented. A tool path adaptation for robotic deburring was presented in accordance with the registration using a custom 3D laser-triangulation profilometer to compensate the positioning errors of the currently processed workpiece, which is difficult to ensure repeatable clamping [27]. A tool path modification method based on a computer-aided design model and direct teaching was proposed to compensate for the position/orientation errors of the workpiece, in addition, impedance control was used to avoid applying an excessive contact force and a virtual wall was adopted to improve the force-control performance for the robotic deburring process [29]. An application of a human mimicking control strategy that mimics the human behavior during the manual deburring on the deburring of hard material items using an industrial robot was introduced [30]. By satisfying a set of constraints to

properly perform the desired surface contact conditioning, a hybrid position/force control approach using task priority and sliding mode control was proposed for contact-driven robotic surface treatments such as deburring [31,32]. A set of optimal process parameter combination for robotic machining and the effect of process parameters such as spindle speed, feed rate and tool path strategies on the performance characteristics were investigated using the Taguchi–Grey relational approach and analysis of variance [33]. Edge robotic deburring with a controlled force progression pneumatic tool, as well as a methodology used to select and optimize the edge robotic deburring process, was presented [25]. A sliding mode control method based on radial basis function neural network was proposed for the deburring of industry robotic systems, without the requirements for strict constraints, an accurate model and exact parameters [34]. A fuzzy proportional–integral–derivative (PID) control method for deburring industrial robots was proposed and the PID controller parameters can be updated online at each sampling time to allow adaptive compensation for error and guarantee trajectory accuracy of the end-effector [35]. A vision-based approach, a Pythagorean hodograph quintic spline interpolator based on S curve acceleration/deceleration and an integrated process control structure consisting of an adaptive disturbance compensator, a sliding mode controller, and a friction compensator were investigated for force control and contour following in industrial applications such as deburring [36].

These studies of tool path adaptation and process parameter control for robotic deburring are usually conducted on one or more traditional and commercial six-DOF serial industrial robot manipulators. The tool path adaptation for robotic deburring implemented usually needs to supplement extra equipment or processes, e.g., using a vision system described in [27,36] or direct teaching [29]. Other studies on the process parameter control for robotic deburring have certain constraints, e.g., the deburring tool is an abrasive diamond disc in the control strategy for the process parameter control, and other deburring tools are not considered [30]; the designed control action and implementation are more intricate, such as [25,31,32,34,36]; the procedure of the proposed approach is more complicated, such as [33]; or detailed deburring process parameters such as robotic feed and spindle speed for the deburring industrial robot are not considered [35].

The deburring orientation adjustment of current industrial robots is usually not dexterous, especially at the far deburring position while simultaneously considering obstacle avoidance. There is an urgent need to develop a robot manipulator for robotic deburring of complex shaped parts with highly dexterous manipulation and very efficient five-face deburring in one setup. Moreover, there are very few related references for the tool path strategies which are implemented as proprietary software packages of robot manufacturers. It is particularly necessary to conduct the research on the tool path planning which is highly suitable for the deburring characteristics of the self-developed robot manipulator. Also, in order to perform an adaptive deburring process and finer deburring quality, it is very important to investigate an easy-to-implement and efficient process parameter control method with automatic-online errors correction.

The rest of this article is organized as follows. The structure of the robot manipulator and related research are described in Section 2. A robotic deburring tool path planning method and a robotic deburring process parameter control method are proposed for robotic deburring in Sections 3 and 4, respectively. A dexterous manipulation verification experiment is presented in Section 5. Two robotic deburring experiments, disc deburring experiment of an automobile hub and multifaceted edges deburring experiment of an automobile steering booster housing, are conducted in Section 6. Finally, conclusions are drawn in Section 7.

2. Structure Description and Related Research of the Robot Manipulator

This section outlines the structure, experimental platforms and previous theoretical research of a developed five-degree-of-freedom (five-DOF) hybrid robot manipulator. The structure of the robot manipulator is shown in Figure 1. The robot manipulator, consisting of a 3-DOF (3T) parallel module and a 2-DOF (2R) serial module, is a newly developed 3T2R hybrid robot manipulator. The first three translational motion axes J_1 , J_2 and J_3 (consisting of ball screws) are driven by motor M_1 , M_2 and M_3 ,

respectively. The last two rotational motion axes J_4 and J_5 are driven by motor M_4 and M_5 , respectively. The axis J_6 is the end-effector which contains a high-speed motor spindle. The designed structure parameter e is equal to zero, and the available range of the rotation angle is $\alpha \in [-\pi/4, \pi/4]$ because of the mechanical constraints.

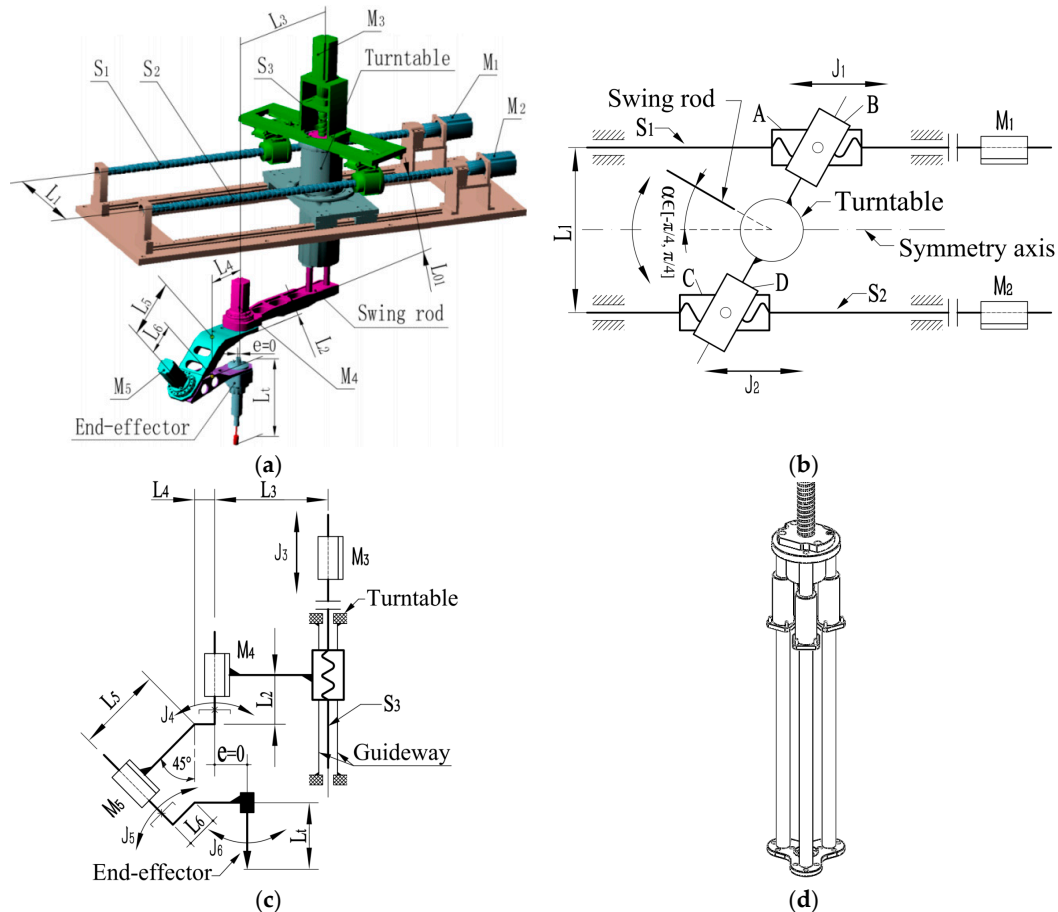


Figure 1. Robot manipulator: (a) 3D model; (b) top view; (c) front view; (d) guideway module.

One of the most significant advantages of the robot manipulator is its dexterity in manipulation and orientation reachability. The last two rotational motion axes J_4 and J_5 as shown in Figure 1 are connected with an angle of 45° in order to realize the dexterous manipulation and the orientation adjustment of the robot manipulator end-effector. The end-effector can reach all orientations in the upper half of the complete spherical surface. Hence, the robot manipulator has the five-face machining ability in one setup. The detailed realizations are described as follows.

When the processing point of the end-effector coincides with the intersection of axes J_4 and J_5 , the position of the processing point of the end-effector can always keep at a same point (i.e., this point always coincides with the intersection), during the process of orientation adjustment in the upper half of the complete spherical surface only through the last two axes J_4 and J_5 . And the position of the processing point can be adjusted when translating the first three axes J_1 , J_2 and J_3 . This means that the manipulation and the orientation reachability of the robot manipulator characterize a very high level of dexterity.

It is necessary to note that some nonnegligible dynamic effects which caused by backlash of ball screws and robot manipulator structural deformations. It is very meaningful to investigate these effects of the backlash and structural deformations and to compensate for them if necessary. Some related research can be referred to [37–40].

Experimental platforms of the robot manipulator are shown in Figure 2. Among them, the improved platform is superior to the original one in mechanical structure on translational vertical axis assembly. The cylinder guide pillar module (shown in Figure 3c) of the improved platform, and the guideway module (shown in Figure 1d) of the original one, are constituted by cylinder guide pillar and cylinder type support, and three sets of linear shafts and linear bearings, respectively. The former has greater torsional rigidity and strength of the vertical axis assembly around the vertical rotation axis than the latter. Finally, design structure and physical structure of the vertical axis assembly for the improved platform are shown in Figure 4.

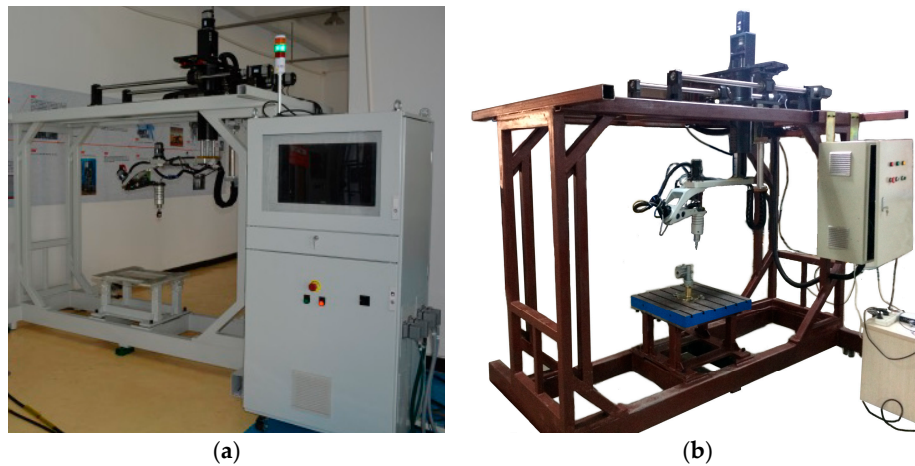


Figure 2. Experimental platforms of robot manipulator: (a) original platform; (b) improved platform.

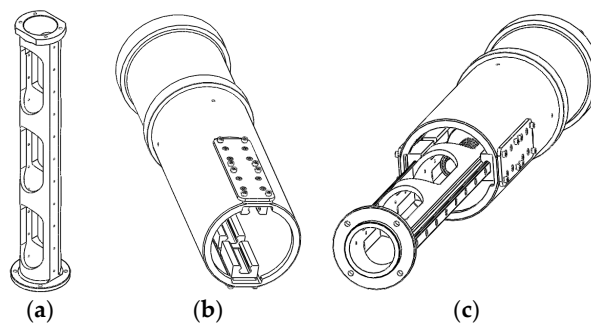


Figure 3. Improved cylinder guide pillar module: (a) cylinder guide pillar; (b) cylinder type support; (c) design structure diagram.

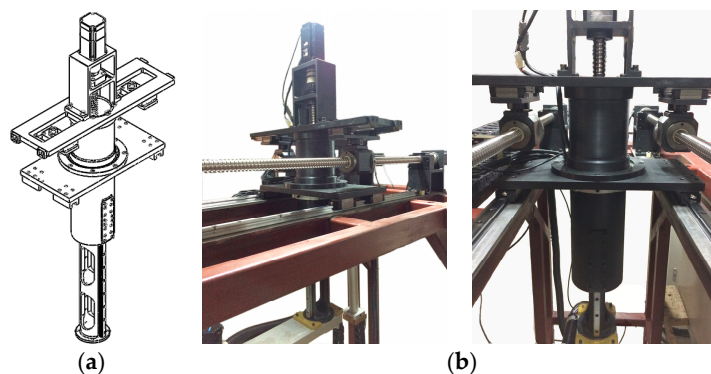


Figure 4. Vertical axis assembly of the improved platform: (a) design structure; (b) physical structure.

The reachable workspace of the robot manipulator based on structure parameters (Table 1) is shown in Figure 5. The top view and the front view of Figure 5 showed the range in the X, Y, and Z

direction of the reachable workspace. Note that the shapes of the left end and the right end (in the top view of the Figure 5) are different. This is caused by the sway of the swing rod. The sway values are $L_3\cos\alpha$ and $L_3\sin\alpha$ in the X and Y directions, respectively. In the start phase, α increases from zero to the maximum attainable value ($\pm\pi/4$), and the sway value in the X and Y directions gradually decrease and increase, respectively. In the end phase, α decreases from the maximum attainable value ($\pm\pi/4$) to zero, and the sway values in the X and Y directions gradually increase and decrease, respectively. The mutual variation relationship is shown in Figure 5a.

In the previous research, kinematics analysis, dynamics analysis, dexterity analysis, multi-objective smooth trajectory planning and dynamic load-carrying capacity calculation, actual building of mechanical system and motion control system, and tests for the repeatability and accuracy of both the position and path for the five-DOF robot manipulator are conducted. For discussions of these domains and a more detailed listing of related research for the robot manipulator, see [41–44].

Table 1. Robot manipulator structure parameters (mm).

L_1	L_2	L_3	L_4	L_5	L_6	e	L_t	L_{01}	s_x/s_z
420	50	450	160	210	95	0	297	465	10

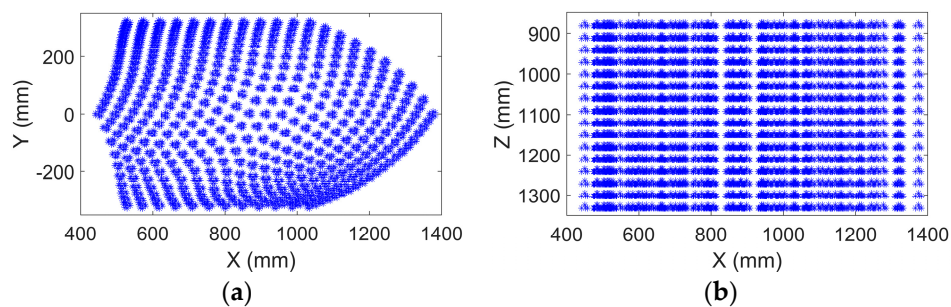


Figure 5. Reachable workspace of robot manipulator: (a) top view; (b) front view.

3. Robotic Deburring Tool Path Planning Method

In this section, a robotic deburring tool path planning method is proposed to handle the robotic deburring tool location (position and orientation) planning and the robotic layered deburring planning for the developed five-DOF robot manipulator.

In this article, the theoretical curve and theoretical surface, which are expected to be qualified after the final robotic deburring, are called the target curve and target surface, respectively. The deburring tool is a general term for various deburring tools, including the cutting tool with the end or side face edge, and the grinding tool such as grinding wheel head and rotary file.

3.1. Robotic Deburring Tool Planning Method

The proposed robotic deburring tool position planning method is discussed in two parts: surface deburring and curve deburring. In the first part (i.e., surface deburring), the tool contact path intersection line method [45] is used to generate the contact position of the deburring tool, i.e., the total locus of deburring tool contact points are derived from the intersection of a set of equidistant constraint planes and the target surface. Among them, the constraint plane spacing, the line spacing and step length of the tool path should be determined by some comprehensive factors such as deburring tool, deburring accuracy, deburring efficiency and deburring error. In the second part, i.e., curve deburring, the above comprehensive factors are also considered to directly generate the total locus of discrete deburring tool contact points. Upon obtaining the total locus of deburring tool contact points for surface deburring and curve deburring, considering the curvature variations of the surface and the curve, respectively, the total locus of deburring tool contact points is offset according to the layered

deburring planning. After that, the deburring tool path of each layer is generated with some practical considerations of deburring tool length, blade edge and blade diameter, etc.

In this article, the orientation of the deburring tool is aligned with its side edge, defined as follows. Deburring tool orientations, the movement direction of the tool and the end edge of the tool are expressed as vectors \mathbf{n} , \mathbf{o} and \mathbf{a} , respectively. A target curve is used as an example to illustrate the robotic deburring tool orientation planning method. The target curve is shown in Figure 6, and unit tangent vectors $\boldsymbol{\tau}$ and unit inner normal vectors \mathbf{f} of discrete positions are represented by blue arrows and green arrows, respectively.

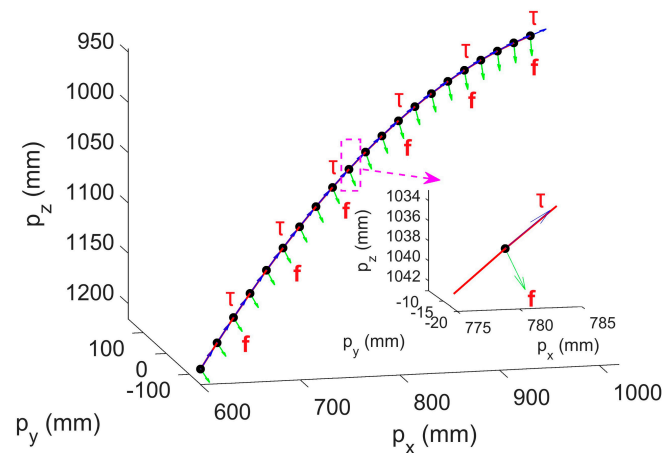


Figure 6. Example of unit tangent and normal vectors for discrete positions of target curve.

The proposed robotic deburring tool orientation planning method is proposed for deburring manners with the tool end edge and the tool side edge. The assignment of orientation vectors for these two deburring manners is described as follows. For the tool end edge (i.e., the deburring manner with the tool end edge): (a) the deburring direction of tool is planned along the tool end edge vector \mathbf{a} , which is chosen as the unit inner normal vectors \mathbf{f} of each discrete position of the target curve; (b) the movement direction of tool (vector \mathbf{o}) is planned along the unit tangent vectors $\boldsymbol{\tau}$ of each discrete position of the target curve and points to the next discrete position to be deburred; and (c) the tool vector \mathbf{n} is obtained by $\mathbf{n} = \mathbf{o} \times \mathbf{a}$. For the tool side edge (i.e., the deburring manner with the tool side edge): (a) the deburring direction of tool is planned along the tool side edge vector \mathbf{n} , which is chosen as the unit inner normal vectors \mathbf{f} of each discrete position of the target curve; (b) the planned movement direction of tool (vector \mathbf{o}) is the same as above deburring manner; and (c) the tool vector \mathbf{a} is obtained by $\mathbf{a} = \mathbf{n} \times \mathbf{o}$.

In the above robotic deburring tool orientation planning, the feeding direction of the robot manipulator deburring corresponds to the deburring tool direction of the end edge or the side edge, that is, the feeding directions of the robot manipulator deburring along the unit inner normal vectors \mathbf{f} for discrete positions of the target curve. The movement direction of the robot manipulator deburring corresponds to the movement direction of the tool, that is, the movement directions of the robot manipulator deburring along the unit tangent vectors $\boldsymbol{\tau}$ for discrete positions of the target curve.

3.2. Robotic Layered Deburring Planning Method

The feature points on the object are selected based on the geometric characteristics of the deburring target, and the machining allowances are measured by the distance between each selected feature point and the target curve and/or surface. The detailed description of the proposed robotic layered deburring planning method for the layered deburring curve and/or surface is presented in the following steps:

Step 1: calculate the distance between each selected feature point and the target curve and/or surface, and find out the maximum one (which is denoted as D_{max}) as the maximum machining allowance for the layered deburring curve and/or surface.

Step 2: calculate the number of deburring layers n (i.e., the times of layered deburring) by the formula $n = \langle D_{\max}/d_p + 1 \rangle$, where d_p and symbolic form $\langle \bullet \rangle$ represent the thickness of each selected deburring layer (i.e., cutting depth) and the rounding calculation, respectively. In order to improve the deburring quality, the deburring count is calculated based on different allowance d_l in the last layer: (a) set it to one when $d_l < d_p/2$ and the deburring allowance sets d_l , and (b) set it to two when $d_l \geq d_p/2$, here, the first deburring allowance sets $d_p/2$, and the second one sets the remains (i.e., $d_l - d_p/2$).

Step 3: plan the deburring tool path on each layer (i.e., the total locus of deburring tool contact points between the deburring tool and the object) based on the index of each layer n_j and its corresponding thickness d_{p-j} , that is, calculate the position offset relationship of each layer for points of the deburring tool path along the outward normal vector $\mathbf{n}_l = [n_{lx} \ n_{ly} \ n_{lz}]^T$ of each discrete point derived from the target curve and/or surface (i.e., the deburring tool contact positions on the target curve and/or surface are obtained by the tool contact path intersection line method [45]), as follows:

$$\begin{bmatrix} x \\ y \\ z \end{bmatrix}_{n_j} = \begin{bmatrix} x \\ y \\ z \end{bmatrix}_{n_{j-1}} + \begin{bmatrix} \Delta x \\ \Delta y \\ \Delta z \end{bmatrix}_{n_j} \quad j = 1, 2, \dots, n, \tag{1}$$

where, when $j = 1$, n_0 and $[x \ y \ z]_{n_0}^T$ represent the number of located layer of the target curve and/or surface and positions of each discrete point of the target curve and/or surface, respectively. And the incremental position calculation is related by

$$\begin{bmatrix} \Delta x \\ \Delta y \\ \Delta z \end{bmatrix}_{n_j} = d_{p-j} \cdot \begin{bmatrix} n_{lx} \\ n_{ly} \\ n_{lz} \end{bmatrix}. \tag{2}$$

Step 4: conduct the semi-finishing and finishing based on actual and special requirements according to Step 2 and Step 3.

Step 5: introduce the orthogonal overlapping and reciprocating manner, and the shape of the basic body surface that is connected with the target curve to conduct planning the deburring tool path for surface deburring and curve deburring at each layer.

In the above-mentioned deburring tool path planning for surface deburring and curve deburring, if the feature points of the object are unknown beforehand, the maximum machining allowance D_{\max} can be estimated by the robot manipulator teaching according to the actual workpiece to be deburred, and the remaining planning steps are the same as above.

Usually, the loci of deburring tool contact points, which are obtained by only using the offset computed from the tool contact path intersection line method [45], may cause a large machining error due to the equal-distance offset. Compared with this tool contact path intersection line method [45], the proposed robotic deburring tool planning method for tool position and tool orientation in this section further extends to consider the curvature variations of the surface and the curve on the basis of this tool contact path intersection line method with the equal-distance offset, so as to ensure a more uniform deburring tool trajectory and repair these deficiencies caused by this method [45].

Please refer to the related documents for detailed explanation of machining mechanism and machining principles for topics such as deburring tool selection and its corresponding robotic deburring feed speed and tool spindle speed for different deburring workpieces with different curves or curves.

4. Robotic Deburring Process Parameter Control Method based on Fuzzy Control

A robotic deburring process parameter control method of the five-DOF robot manipulator for robotic deburring is proposed in this section. This proposed method is adopted in deburring process parameter adjustment control for the stable robotic deburring with a constant cutting speed and a constant cutting force via a designed fuzzy controller.

According to metal cutting principle, the cutting parameters include cutting speed, cutting feed and cutting depth. Taking carbide turning tools for carbon steel turning as an example, related researches showed that the biggest impact on tools is the cutting speed, followed by the cutting feed, and lastly the cutting depth [46–48]. More generally, the rough machining should select cutting parameters for the maximum productivity. Thus, a larger cutting depth (or cutting width) should be selected first, and after the majority of the machining allowance is removed, a suitable cutting feed (or a cutting thickness) and a cutting speed are selected in turn by the cutting condition. Finish machining generally uses a small cutting depth and cutting feed, and then a higher cutting speed to improve the machining accuracy and reduce the surface roughness.

In this article, robotic deburring process parameters—robotic spindle speed, robotic feed and robotic layered deburring thickness—are determined by cutting parameters—cutting speed, cutting feed and cutting depth—respectively. Among them, the robotic layered deburring thickness (i.e., cutting depth) planning and the robotic deburring tool location (position and orientation) planning are presented in the proposed robotic deburring tool path planning method in Section 3. In this section, issues to consider here pertain, mostly, to the adjustment control for robot manipulator deburring process parameters, that is robotic spindle speed and robotic feed, through a proposed robotic deburring process parameter control method.

Some classical control methods, such as proportional–integral–derivative (PID) control, which have been studied and practiced by broad researches, are very effective solutions for uncomplicated linear time-invariant systems [49–51]. In addition, modern control theory, such as sliding mode control, based on state variables has also been widely used to solve linear or nonlinear, and time-invariant or time-varying multi-input multi-output (MIMO) systems [52–54]. Although this kind of classical and modern control theory can overcome some internal disturbances of the control system, nevertheless, it is neither sufficient to ensure the stability of robotic deburring process in a robust enough way in real time, nor able to cope with environmental uncertainties. One goal of this article is to find a way of controlling the robotic deburring contact forces while maintaining constant cutting speed and cutting force of the robot manipulator presented earlier. In particular, this is critical when the interaction between the robot manipulator and deburring workpiece environment is of concern.

Because the fuzzy control with the ontological basis of fuzzy logic and fuzzy reasoning has the advantage of requiring neither the knowledge of the model structure nor the model parameters, it is strongly adaptive and highly robust to nonlinearity and variations of process parameters. Also, it can give fast response, effective noise suppression, and a better control effects when the model structure changes greatly. Therefore, related researches and applications based on fuzzy control have been favored by many scholars [55–58].

In this article, the process of the adjustment control for robot manipulator deburring process parameters (i.e., robotic spindle speed and robotic feed) has the characteristics of nonlinearity, noise and tight coupling between control loops, which cannot be solved sufficiently by classical and modern control methods such as PID-type controllers. In this section, a fuzzy controller with the above advantages of the fuzzy control is designed for a proposed robotic deburring process parameter control method to systematically accommodate robotic deburring.

The control objectives of the designed fuzzy control system in this section are the robot manipulator deburring process parameters, i.e., robotic spindle speed and robotic feed. The robotic spindle speed and the robotic spindle load of the robot manipulator deburring system can be controlled by adjusting the control voltage of the robotic spindle and the robotic feed, in order to realize the robotic deburring with a constant cutting speed and a constant cutting force. Hence, the designed fuzzy controller in this section is a two-input and two-output control system (shown in Figure 7). Here, input variables are robotic spindle speed and robotic spindle load, and output variables are control voltage of the robotic spindle and robotic feed.

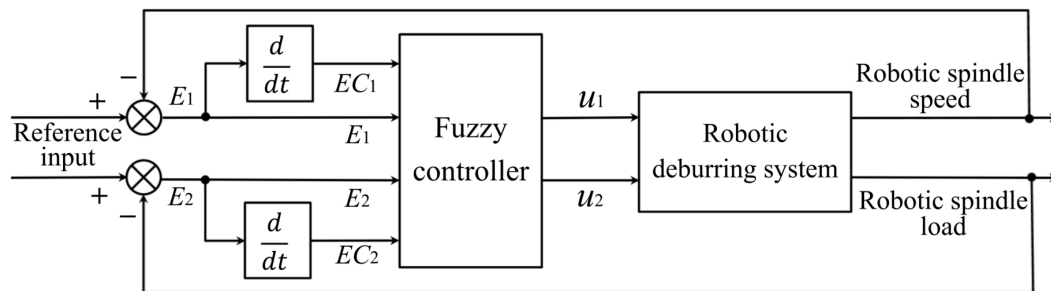


Figure 7. Schematic diagram for deburring process parameter control.

In this article, a parallel structure adopted is used by the fuzzy controller to independently control the control voltage of the robotic spindle and the robotic feed. There are two parts of representing fuzzy variables in the designed fuzzy controller. First, error of robotic spindle speed E_1 and change in error of robotic spindle speed EC_1 , and error of robotic spindle load E_2 and change in error of robotic spindle load EC_2 , are represented as input fuzzy variables for controlling the control voltage of the robotic spindle and the robot feed, respectively. Second, change in control voltage of the robotic spindle u_1 and change in robotic feed u_2 are represented as output fuzzy variables.

To achieve discrete membership functions, a discrete set with thirteen elements and a discrete set with seven elements are defined in the designed fuzzy controller for E_1, EC_1 , and u_1 , and for E_2, EC_2 , and u_2 , respectively, and corresponding sets are $U_1 = \{-6 \ -5 \ \dots \ -1 \ 0 \ +1 \ +2 \ \dots \ 6\}$ and $U_2 = \{-3 \ -2 \ -1 \ 0 \ +1 \ +2 \ +3\}$, respectively. Assume that variation ranges of E_1, EC_1, E_2 and EC_2 are $[-S_e, S_e], [-S_{ec}, S_{ec}], [-L_e, L_e]$ and $[-L_{ec}, L_{ec}]$, respectively. Combining these variation ranges and corresponding discrete sets, several quantizers corresponding to E_1, EC_1, E_2 and EC_2 are defined respectively as follows:

$$K_{S_e} = 6/S_e, \tag{3}$$

$$K_{S_{ec}} = 6/S_{ec}, \tag{4}$$

$$K_{L_e} = 3/L_e, \tag{5}$$

$$K_{L_{ec}} = 3/L_{ec}. \tag{6}$$

Here, each quantizer maps an inbound measurement within the variation range to a nearest integer element in the corresponding discrete set.

Similarly, scaling factors for the output variables (i.e., control variables) of u_1 and u_2 , where corresponding variation ranges are $[-V_u, V_u]$ and $[-F_u, F_u]$, respectively, are defined as follows:

$$K_{V_u} = V_u/6, \tag{7}$$

$$K_{F_u} = F_u/3. \tag{8}$$

Assuming exact values obtained by the fuzzy reasoning for change in control voltage of the robotic spindle u_1 and change in robotic feed u_2 are u_{1i} and u_{2i} , respectively, then corresponding exact values of variation ranges V_{ui} and F_{ui} can be obtained by using above defined scaling factors. The detailed representations are given by

$$V_{ui} = K_{V_u} \cdot u_{1i}, \tag{9}$$

$$F_{ui} = K_{F_u} \cdot u_{2i}. \tag{10}$$

The fuzzy rule with automatic adjusting factors in the whole set using analytical expressions for fuzzy controller are usually designed as follows. Suppose that sets for error E , change in error EC and control variable u select as $E = EC = u = \{-N, \dots, -2, -1, 0, 1, 2, \dots, N\}$, the fuzzy rule can be expressed as

$$\begin{cases} u = -\langle \alpha E + (1 - \alpha)EC \rangle \\ \alpha = \frac{1}{N}(\alpha_s - \alpha_0)|E| + \alpha_0 \end{cases} \quad (11)$$

where $0 \leq \alpha_0 \leq \alpha_s \leq 1$ and adjustment factor $\alpha \in [\alpha_0, \alpha_s]$, and symbolic form $\langle \bullet \rangle$ represents the rounding calculation. Thus, the designed fuzzy rule can be automatically adjusted on the basis of the weight and magnitude of the error.

In this article, in order to optimize the designed fuzzy controller that provides good both static and dynamic stability properties, and robust performance, fuzzy rules are designed with automatic adjusting factors in the whole set, described by analytical expressions. Thus, in the whole set, weights of errors and changes in errors, which represent the effect on control results, can be automatically adjusted by errors. The detailed fuzzy rules for robotic spindle speed and robotic spindle load are designed respectively as follows:

$$\begin{cases} u_1 = -\langle \alpha_1 E_1 + (1 - \alpha_1)EC_1 \rangle \\ \alpha_1 = \frac{1}{6}(\alpha_{s1} - \alpha_{01})|E_1| + \alpha_{01} \end{cases} \quad (12)$$

where $0 \leq \alpha_{01} \leq \alpha_{s1} \leq 1$ and adjustment factor $\alpha_1 \in [\alpha_{01}, \alpha_{s1}]$, and symbolic form $\langle \bullet \rangle$ represents the rounding calculation; and

$$\begin{cases} u_2 = -\langle \alpha_2 E_2 + (1 - \alpha_2)EC_2 \rangle \\ \alpha_2 = \frac{1}{3}(\alpha_{s2} - \alpha_{02})|E_2| + \alpha_{02} \end{cases} \quad (13)$$

where $0 \leq \alpha_{02} \leq \alpha_{s2} \leq 1$ and adjustment factor $\alpha_2 \in [\alpha_{02}, \alpha_{s2}]$, and $\langle \bullet \rangle$ represents the same mentioned above.

It can be seen from the above that fuzzy rules are characterized naturally in that the adjustment factors α_1 and α_2 can be updated online and adjusted by the absolute value of the error $|E_1|$ and $|E_2|$, and there are six and three possible values, respectively, therefore, weights of errors and changes in errors can be automatically adjusted online by errors.

The automatic adjustment process of the above designed fuzzy rules conforms to the control characteristics of the human decision-making process, and these fuzzy rules described by the analytical forms exhibit their several own advantages over other representations in the optimization property, convenience, simplicity, and implementation in real time for fuzzy control algorithms.

5. Dexterous Manipulation Verification Experiment

In this section, an experiment is conducted on the improved experimental platform of the robot manipulator (shown in Figure 8a) to verify the dexterous manipulation of the robot manipulator, especially the dexterous manipulation of a certain processing point. An aluminum alloy casting automobile steering booster housing (shown in Figure 8b) was selected as the experimental object, and the dexterous manipulation verification experiment was carried out at the center hole on the cylindrical top of the booster housing (shown in Figure 8b).

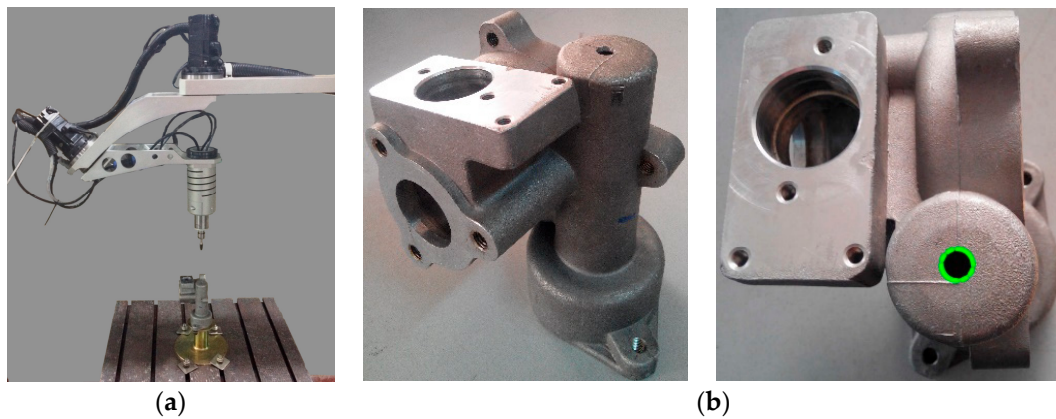


Figure 8. Experimental platform and experimental object: (a) experimental platform of improved robot manipulator; (b) overall appearance of booster housing.

Experimental verification of the dexterous manipulation was carried out on the platform of the improved robot manipulator. When the last two axes J_4 and J_5 both matched the actual initial state (shown in Figure 8a), the first three axes J_1 , J_2 and J_3 were adjusted so that the tool tip of the end-effector reached the center hole on cylindrical top of the booster housing until the intersection of the last two axes J_4 and J_5 basically coincided with the center hole (shown in Figure 8b). Then the first three axes J_1 , J_2 and J_3 remained stationary, and only the last two axes J_4 and J_5 rotated within the motion range. The characterizations of the dexterous manipulation of the robot manipulator are shown in Figure 9. The enveloping surface of the dexterous manipulation verification experiment is shown in Figure 10.

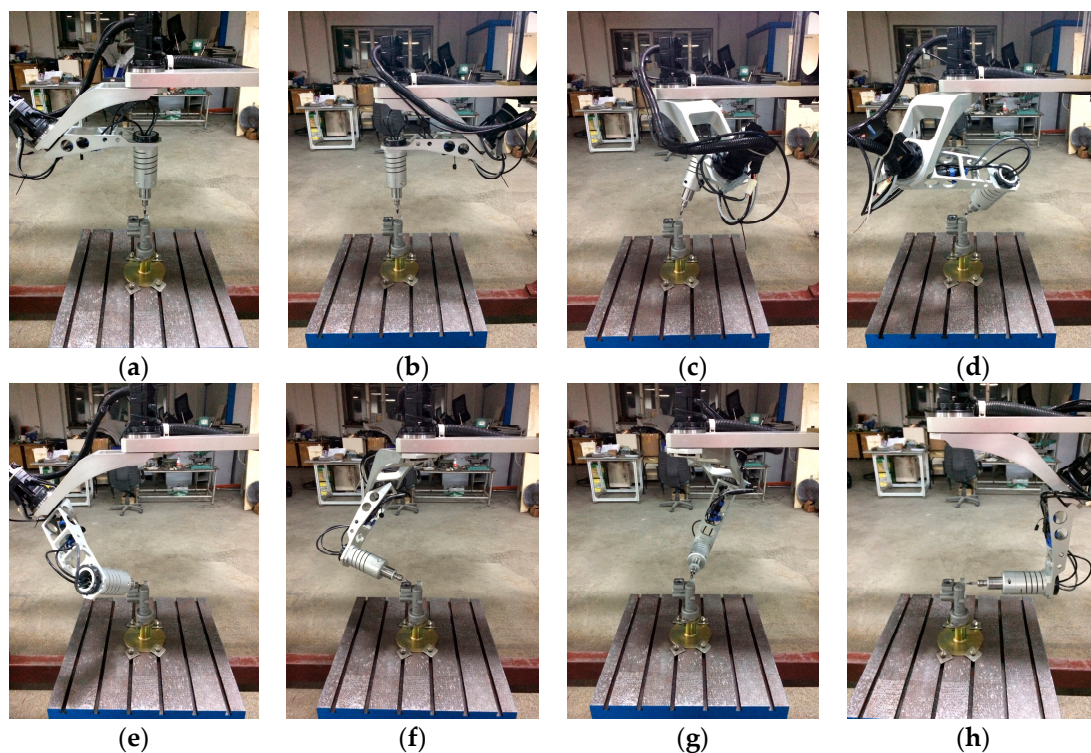


Figure 9. Experimental validation of the dexterous manipulation (unit is radian): (a) $\varphi_4 = 0$, $\varphi_5 = 0$; (b) $\varphi_4 = -\pi$; $\varphi_5 = 0$; (c) $\varphi_4 = -2\pi/3$; $\varphi_5 = \pi/6$; (d) $\varphi_4 = -\pi/6$; $\varphi_5 = \pi/3$; (e) $\varphi_4 = 0$; $\varphi_5 = \pi/2$; (f) $\varphi_4 = \pi/6$; $\varphi_5 = 2\pi/3$; (g) $\varphi_4 = 2\pi/3$; $\varphi_5 = 5\pi/6$; (h) $\varphi_4 = \pi$; $\varphi_5 = \pi$.

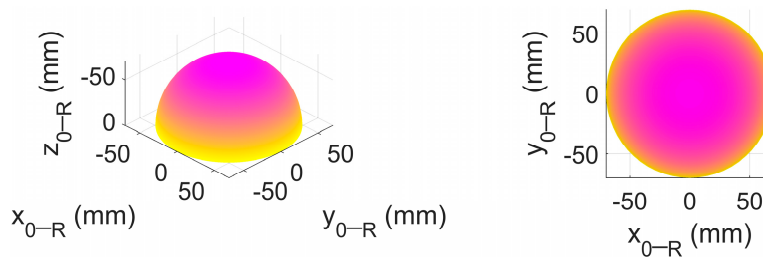


Figure 10. Enveloping surface of the experiment validation for the dexterous manipulation.

When the last two axes J_4 and J_5 traversed the motion ranges $[-\pi, \pi]$ and $[0, \pi]$, respectively, as shown in Figure 9, it can be found that the total locus of the tool tip of the end-effector appeared as an approximate enveloping half-spherical surface with a downward open, as shown in Figure 10, and the center of the half-spherical surface was the intersection of the last two axes J_4 and J_5 . In addition, the total locus of the tool tip remained the same when the last two axes J_4 and J_5 traversed the motion ranges $[-\pi, \pi]$ and $[-\pi, 0]$, respectively. For the sake of simplicity, only the former case is illustrated in Figure 9. Note that the approximate enveloping half-spherical surface was not a strictly half-spherical surface, and the extremely small difference was caused by the structure parameter e , which was not strictly equal to zero due to assembly errors.

The above results of the dexterous manipulation experiment imply that the robot manipulator has a very high level of the dexterous manipulation and the orientation reachability. These available and excellent characterizations of the dexterous manipulation and the orientation reachability can provide appropriate and flexible manipulations and orientation adjustments with a very high level of dexterity for the robotic deburring of the robot manipulator.

6. Robotic Deburring Experiments

Two robotic deburring experiments were conducted on the experimental platforms of the robot manipulator in this section to show the effectiveness of the proposed robotic deburring tool path planning method and the proposed robotic deburring process parameter control method, and also to demonstrate the superiorly operational manipulation performance and the deburring ability of the robot manipulator.

6.1. Disc Robotic Deburring Experiment

In the first robotic deburring experiment, a disc deburring for an automobile hub was conducted on the original experimental platform of the robot manipulator (shown in Figure 2a). The experimental workpiece was an aluminum alloy casting blank of an automobile hub, as shown in Figure 11a, and the experimental deburring object were disc burrs of the automobile hub, as shown in Figure 11b.

It can be seen from Figure 11 that disc burrs of automobile hub were located on the inside of the mold cavity, so that these burrs were not suitable to be removed via the abrasive belt grinding. It was a good use case of a certain carbide rotary tool (i.e., a kind of high-speed machining file, shown in Figure 12) driven by the robot manipulator with a high level of dexterity of manipulation and orientation reachability. Furthermore, this kind of rotary tool with a relatively long side cutting edge is more suitable to execute the deburring for disc burrs of automobile hub. A double-cutting cylindrical round-head carbide rotary tool with the side cutting edge (shown in Figure 12b and its type is CX1020M06) was selected to carry out the deburring for disc burrs of automobile hub in the first experiment. The length of the side cutting edge and the diameter of the selected tool were 20 mm and 10 mm, respectively.



Figure 11. Casting blank of automobile hub: (a) overall appearance of automobile hub; (b) disc burrs of automobile hub.

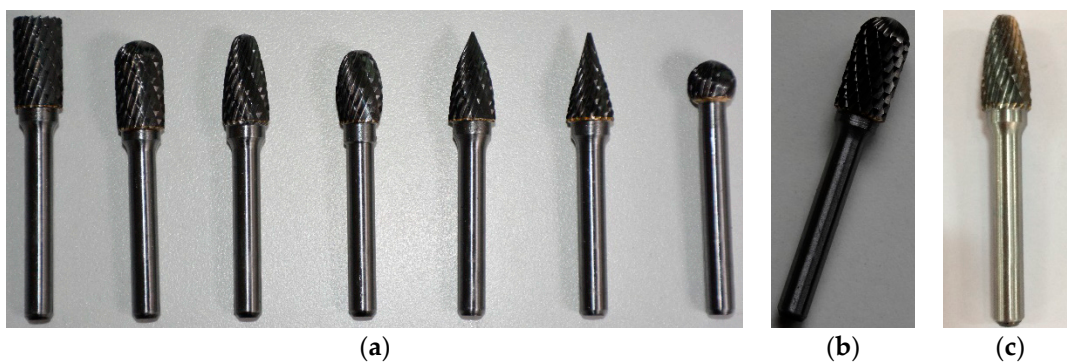


Figure 12. Carbide rotary tools: (a) series of tools; (b) cylindrical ball nose tool; (c) arch ball nose tool.

Based on the proposed robotic deburring tool path planning method, the detailed robotic deburring tool location (position and orientation) planning and the detailed robotic layered deburring planning are presented as follows. The selected tool can deburr once the entire thickness of burrs due to the length of the side cutting edge is significantly larger than the thickness of burrs with range between 0.37 mm and 0.72 mm. Thus, the disc burrs of automobile hub can be removed by executing robotic layered deburring several times through the proposed robotic deburring tool path planning method.

Disc burrs vary in size and exhibit a discontinuous distribution as can be seen in Figure 11b. Through the actual measurement, the maximum width dimension, i.e., the maximum machining allowance D_{\max} was 7.36 mm. In the first experiment, the thickness of the single-layer deburring, i.e., the cutting depth d_p was set as about one third of the diameter of the side cutting edge, which was taken as 3 mm. The entire allowance can be deburred completely by repeating three times. Among them, the thickness of the last deburring layer was selected as 1.36 mm to improve the deburring quality.

Furthermore, a total of eighteen discrete points were selected on the entire target curve at the edge of disc body, as shown in Figure 13. The position of each contact point of the layered deburring tool is planned by the Equations (1) and (2) along the exterior normal \mathbf{n}_i (red arrows are showed in Figure 14a) of each discrete point, as shown in Figure 14a. As mentioned above, disc burrs of the automobile hub were suitable for deburring with the tool side cutting edge and the contact orientations of the layered deburring tool were planned as shown in Figure 14b. The details were: (a) the deburring direction of tool, i.e., the tool side edge vector \mathbf{n} was taken as the unit inner normal vector \mathbf{f} of each discrete position (i.e., cyan arrows, as shown in Figure 14b, and they were in the opposite direction of the red arrows as shown in Figure 14a); (b) the movement direction of tool (vector \mathbf{o}) was planned along the unit tangent vectors $\boldsymbol{\tau}$ of each discrete position (i.e., green arrows, as shown in Figure 14b) and points to the next discrete position to be deburred; and (c) the tool vector \mathbf{a} was derived as $\mathbf{a} = \mathbf{n} \times \mathbf{o}$. Finally, the disc deburring of the automobile hub was conducted in the clockwise direction based on

the planned tool contact positions and tool contact orientations as shown in Figure 14 (symbols ①, ② and ③ represent the sequence of each layered deburring).

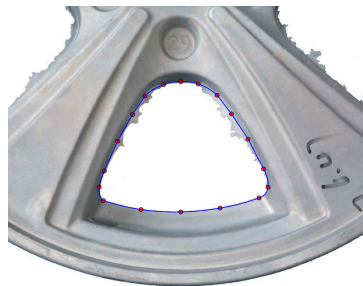


Figure 13. Target curve of disc and discrete points.

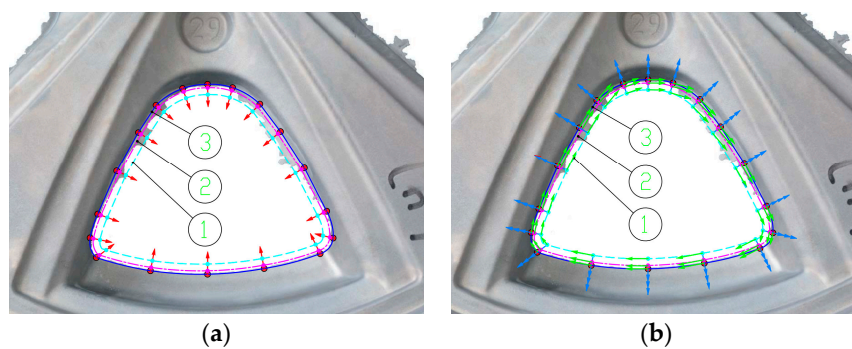


Figure 14. Tool locations planning of the layered deburring: (a) tool contact positions; (b) tool contact orientations.

Additionally, the proposed robotic deburring process parameter control method was applied to the robotic deburring of the first experiment in order to adjust robotic deburring process parameters with a constant cutting speed and a constant cutting force. In this experiment, the robotic spindle speed was selected to be 10,000 rpm, and the line speed of the robotic feed was set to 30 mm/s. Hence, the desired robotic spindle speed and the desired robotic spindle load were 10,000 rpm and 0.17N·m. Variation ranges E_1 , EC_1 , E_2 and EC_2 (corresponding to $[-S_e, S_e]$, $[-S_{ec}, S_{ec}]$, $[-L_e, L_e]$ and $[-L_{ec}, L_{ec}]$, respectively) were set to $[-3000, 3000]$, $[-800, 800]$, $[-0.05, 0.05]$ and $[-0.02, 0.02]$, respectively. Variation ranges of output variables, i.e., change in control voltage of the robotic spindle and change in robotic feed (corresponding to $[-V_u, V_u]$ and $[-F_u, F_u]$, respectively), were set to values such that $[-0.3, 0.3]$ and $[-3, 3]$, respectively. From (3)–(8), quantizers of E_1 , EC_1 , E_2 and EC_2 , and scaling factors of u_1 and u_2 , were obtained as $K_{S_e} = 0.002$, $K_{S_{ec}} = 0.0075$, $K_{L_e} = 60$, and $K_{L_{ec}} = 150$, and $K_{V_u} = 0.05$ and $K_{F_u} = 1$, respectively. Furthermore, adjustment factors α_1 and α_2 were set to $\alpha_1 \in [0.3, 0.7]$ and $\alpha_2 \in [0.2, 0.8]$, respectively. Hence, the fuzzy rules in the designed fuzzy controller for robotic spindle speed and robotic spindle load are expressed respectively as follows:

$$\begin{cases} u_1 = -\langle \alpha_1 E_1 + (1 - \alpha_1) EC_1 \rangle \\ \alpha_1 = \frac{1}{6}(0.7 - 0.3)|E_1| + 0.3 \end{cases} \quad (14)$$

$$\begin{cases} u_2 = -\langle \alpha_2 E_2 + (1 - \alpha_2) EC_2 \rangle \\ \alpha_2 = \frac{1}{3}(0.8 - 0.2)|E_2| + 0.2 \end{cases} \quad (15)$$

The experimental platform and the automobile hub workpiece of the first robotic experimental deburring are shown in Figure 15. The detailed robotic experimental deburring for disc burrs of the automobile hub on the original experimental platform is shown in Figure 16. Results of layered experimental deburring disc of the automobile hub workpiece are shown in Figure 17. Finally, the results of the target planning path and actual tool path of experimental deburring for the automobile hub

workpiece are shown in Figure 18 (here, the blue line and the red line are the target planning path and the actual tool path, respectively). Deviation results of target planning path and actual tool path of experimental deburring for disc of hub are shown in Figure 19, the vertical axis indicates the magnitude of the deviation, and other two horizontal axes in the horizontal plane indicate the corresponding positions of the target planning path in the deburring experiment. In addition, a figure in the form of plane polar coordinates illustrating deviation results of this experiment deburring is shown in Figure 20. The maximum deviation was 1.23 mm, and these robotic deburring results can meet the experimental deburring requirements.

The effectiveness of the proposed robotic deburring tool path planning method and the proposed robotic deburring process parameter control method were verified in the first deburring experiment. Also, it can be seen that the robotic deburring orientations were adjusted dexterously, especially in the place where the local curvature changes greatly, and the dexterous deburring ability of the robot manipulator was fully demonstrated in the first deburring experiment.

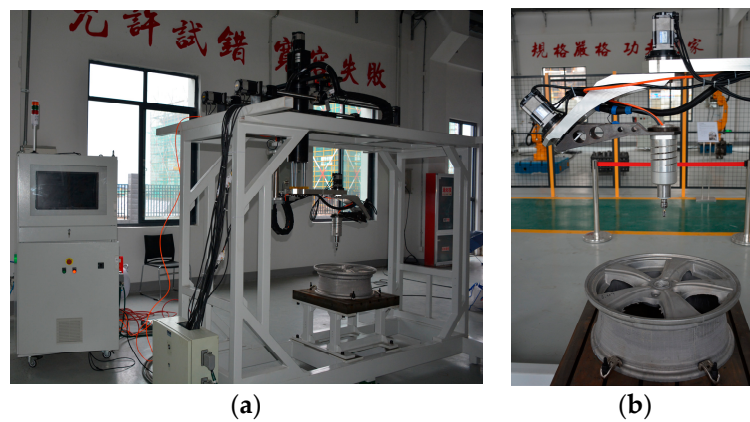


Figure 15. Experimental platform and automobile hub: (a) original experimental platform of robot manipulator; (b) automobile hub workpiece.



Figure 16. Experimental deburring disc of hub on original experimental platform.

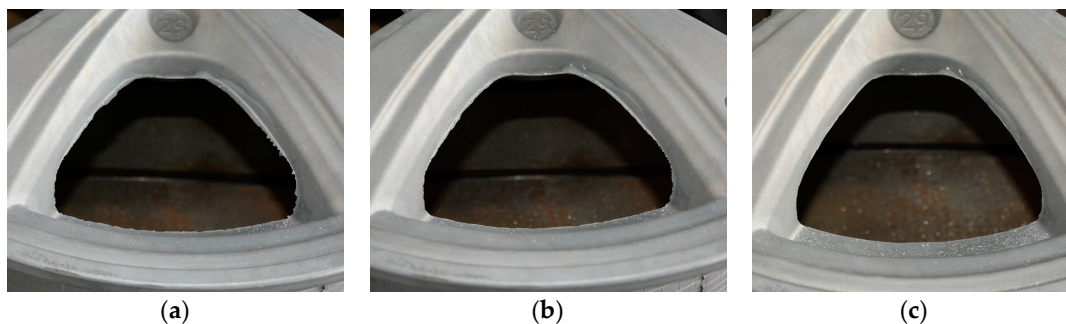


Figure 17. Results of layered experimental deburring disc of hub: (a) first layered deburring; (b) second layered deburring; (c) third layered deburring.

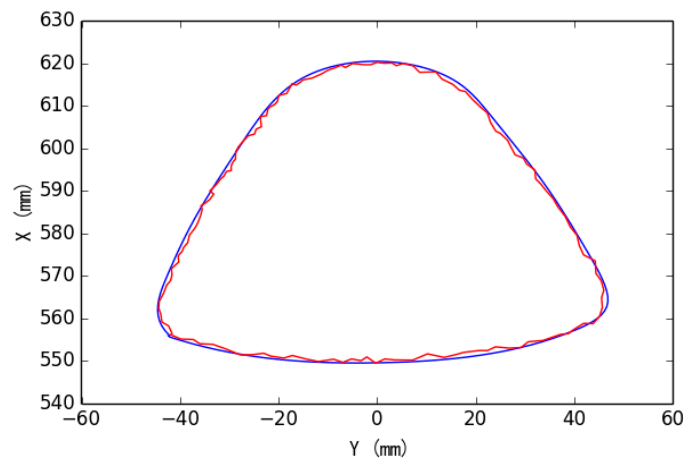


Figure 18. Results of target planning path and actual tool path of experimental deburring.

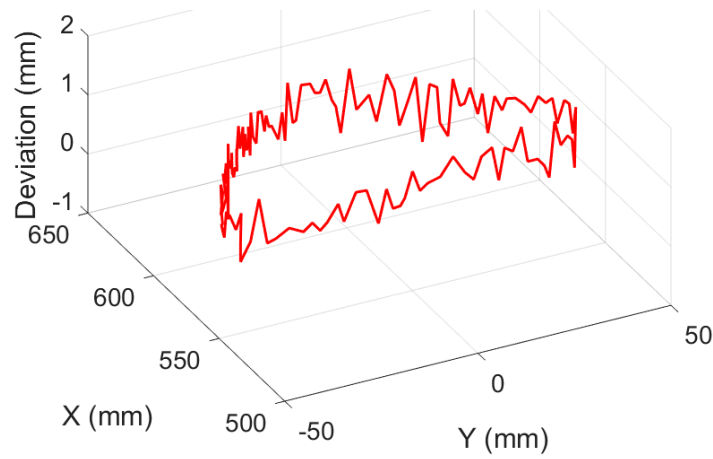


Figure 19. Deviation results of target planning path and actual tool path of experimental deburring for disc of hub.

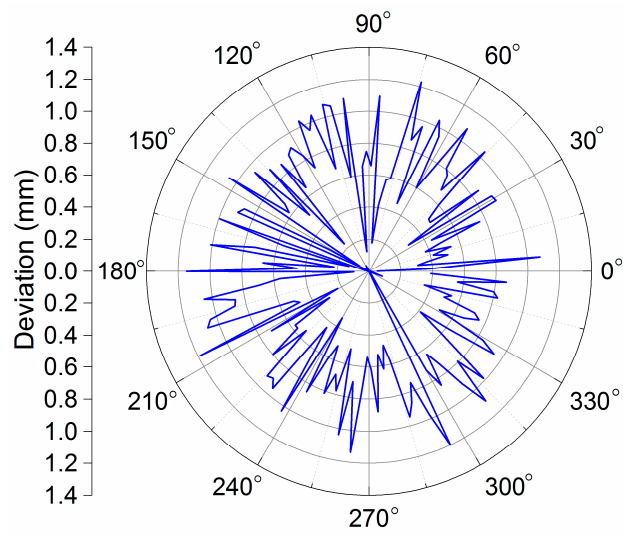


Figure 20. Deviation results of target planning path and actual tool path of experimental deburring for disc of hub (polar representation).

6.2. Multifaceted Edges Robotic Deburring Experiment

In the second robotic deburring experiment, multifaceted edges deburring for an automobile steering booster housing were conducted on the improved experimental platform of the robot manipulator (shown in Figures 2b and 8a). The experimental object was an aluminum alloy casting automobile steering booster housing (shown in Figure 8b), and the experimental deburring object were multifaceted edges of the automobile steering booster housing, as shown in Figure 21, i.e., orifice edges (blue lines are showed in Figure 21) and facet edges (red lines are showed in Figure 20) on top facet, distal side facet and proximal side facet relative to the initial position of the robot manipulator, as shown in Figure 21a,b,c, respectively.

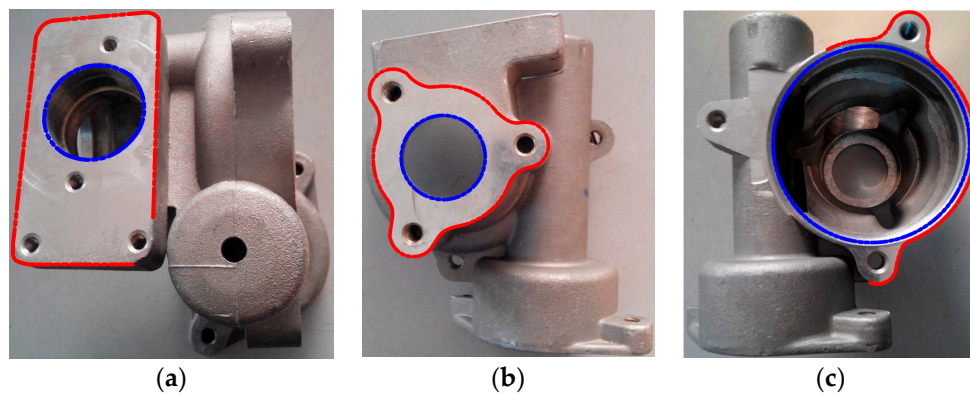


Figure 21. Experimental deburring of multifaceted edges for automobile steering booster housing: (a) top facet; (b) distal side facet; (c) proximal side facet.

A double-cutting arch round-head carbide rotary tool with the side cutting edge (shown in Figure 12c and its type—FX1020M06) was selected to conduct the deburring for multifaceted edges of automobile steering booster housing in the second experiment. In the multifaceted edges deburring experiment, the planned movement directions of the robotic deburring tool were clockwise and counterclockwise for orifice edges deburring and facet edges deburring, respectively.

Since burrs on multifaceted edges are very small, the entire allowance of each facet edge burrs could be deburred completely only once. Similarly, the proposed robotic deburring tool path planning method and the proposed robotic deburring process parameter control method were applied as in the first deburring experiment. Among them, the robotic spindle speeds for orifice edges deburring and facet edges deburring are selected to be 10,000 rpm and 8000 rpm, respectively; and the line speeds of the robotic feed for top facet edges deburring and other edges deburring were set to 30 mm/s and 20 mm/s, respectively. Note that these selected values for robotic spindle speeds and robotic feed speeds are not guaranteed to be very suitable as they are selected only according to limited past experiences. As mentioned above, the most appropriate way of selecting extremely suitable robotic deburring feed speed and tool spindle speed for specific deburring workpiece needs to refer to some related research issues for the technical details and be verified by a series of deburring experiments.

The detailed robotic experimental deburring for orifice edges and facet edges on the top facet, distal side facet and proximal side facet are shown in Figures 22 and 23, Figures 24 and 25, and Figures 26 and 27, respectively. Finally, experimental deburring results for multifaceted edges of the automobile steering booster housing are shown in Figure 28. And robotic experimental deburring results of target planning path and actual tool path of top facet, distal side facet and proximal side facet are shown in Figures 29–31, respectively (here, the blue line and the red line are the target planning path and the actual tool path, respectively). Deviation results of target planning path and actual tool path of robotic experimental deburring for top facet, distal side facet and proximal side facet are shown in Figures 32–34, respectively. In each deviation figure, the vertical axis indicates the magnitude of the deviation, and other two horizontal axes in the horizontal plane indicated the corresponding positions

of the target planning path in the deburring experiment (here, the blue line and the red line are the facet edges deburring deviation results and the orifice edges deburring deviation results, respectively). In addition, three figures in the form of plane polar coordinates illustrating deviation results of this experiment deburring for top facet, distal side facet and proximal side facet are shown in Figures 35–37, respectively. Among them, the maximum path deviations of top facet edge, distal side facet edge and proximal side facet edge were 0.97 mm, 1.13 mm and 1.21 mm, respectively. These robotic deburring results can satisfy the experimental deburring requirements.

It can be showed that the effectiveness of the proposed robotic deburring tool path planning method and the proposed robotic deburring process parameter control method were also verified in the second deburring experiment. Furthermore, the highly efficient and dexterous manipulation and deburring capacity of the robot manipulator for multifaceted deburring in one setup was totally demonstrated in the second deburring experiment. In addition, it should be noted that the proposed methods can be now only applied to soft material machining applications and low machining requirements due to the rigidity defect of the robot manipulator and lacking compensation for vibrations and/or chattering, although it had a very high level of dexterous manipulation and orientation reachability. There are still many meaningful research issues need to be conducted in the next step in order to improve the path accuracy of the robot manipulator, such as offline path correction, compensation for vibrations and/or chattering, high frequency oscillation suppression, structural rigidity improvement, calibration of the robot manipulator for dealing with nonnegligible dynamic effects which are caused by backlash of ball screws and robot manipulator structural deformations.

It is necessary to note that, when the end-effector tool of the robot manipulator is changed, like an abrasive belt or a fabric wheel, the robot manipulator can also conduct deburring, grinding and polishing for edges and surfaces of castings or other materials, such as parting line burrs, flash burrs, pouring risers burrs, and so forth.

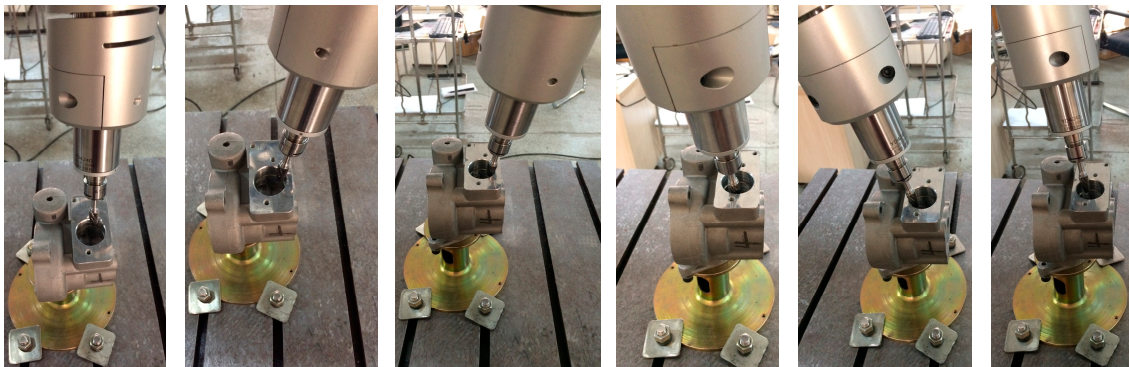


Figure 22. Experimental deburring of orifice edges on top facet.



Figure 23. Experimental deburring of facet edges on top facet.

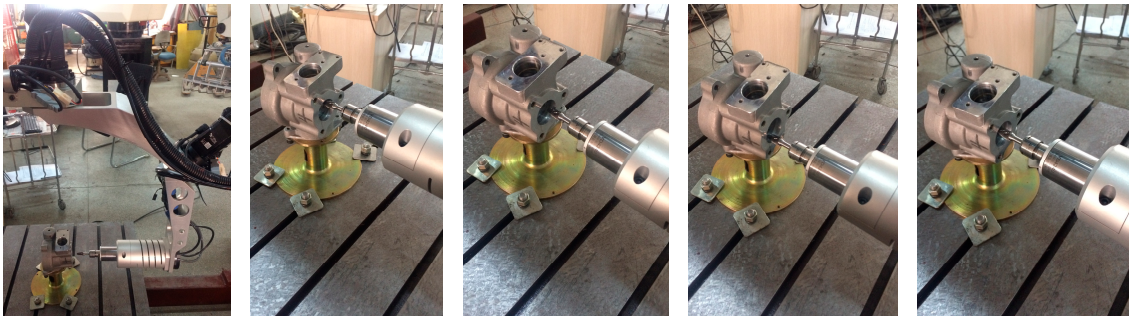


Figure 24. Experimental deburring of orifice edges on distal side facet.

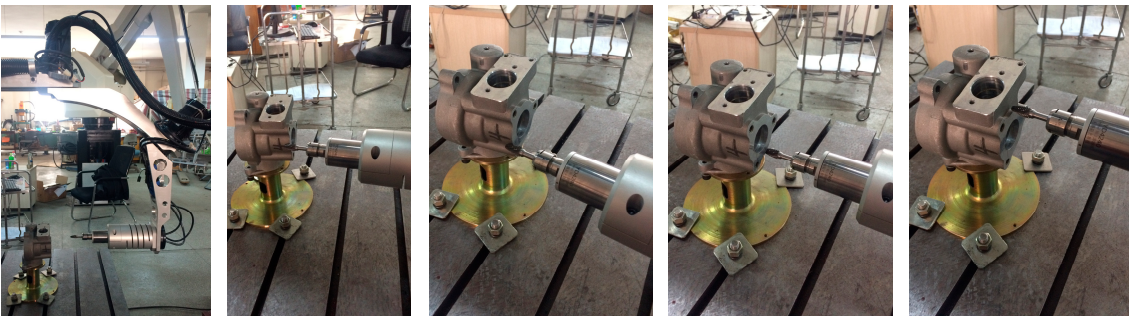


Figure 25. Experimental deburring of facet edges on distal side facet.

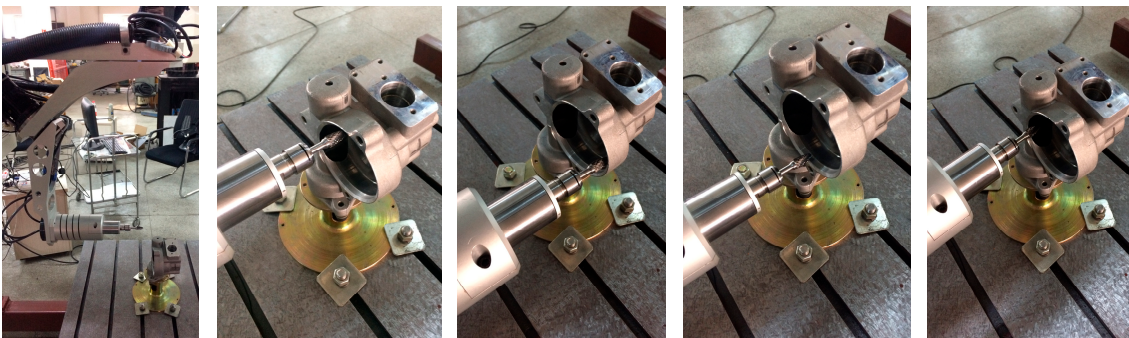


Figure 26. Experimental deburring of orifice edges on proximal side facet.

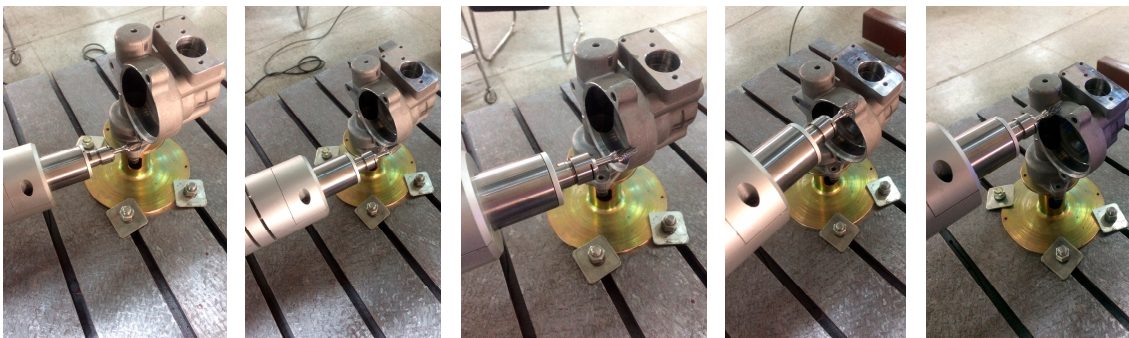


Figure 27. Experimental deburring of facet edges on proximal side facet.

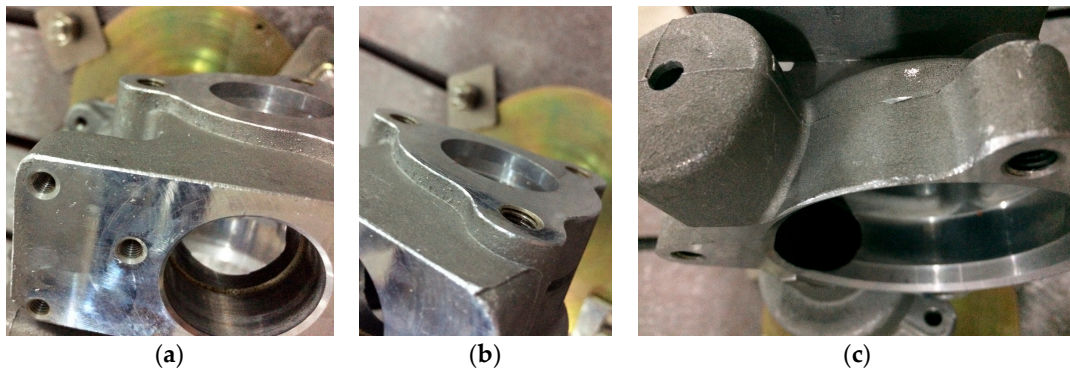


Figure 28. Experimental deburring results for multifaceted edges of automobile steering booster housing: (a) top facet; (b) distal side facet; (c) proximal side facet.

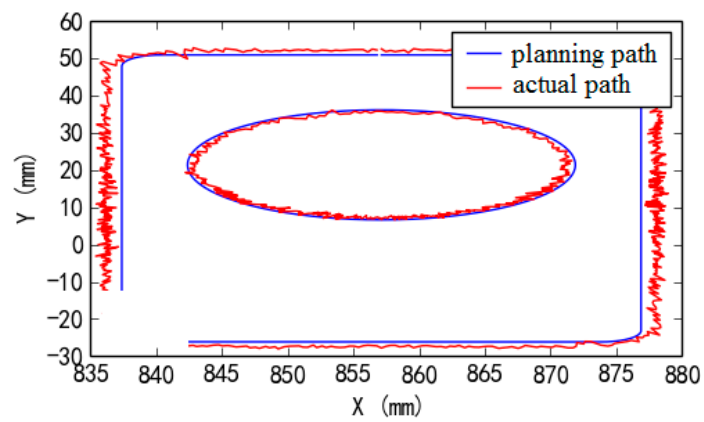


Figure 29. Experimental deburring results of target planning path and actual tool path of top facet.

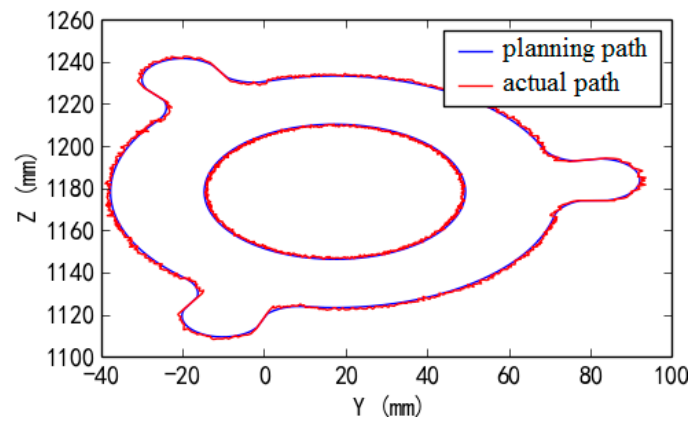


Figure 30. Experimental deburring results of target planning path and actual tool path of distal side facet.

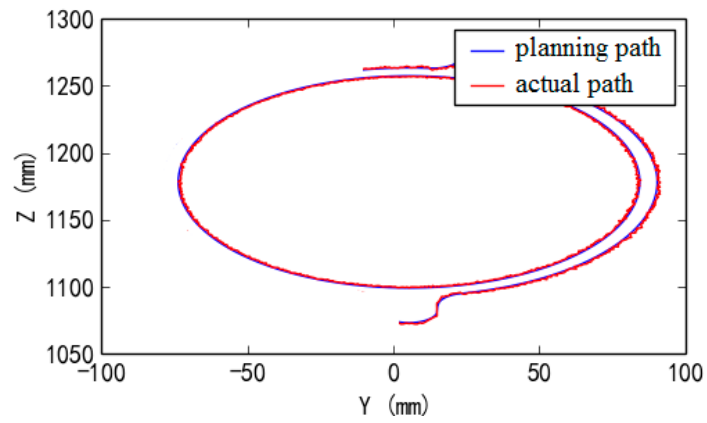


Figure 31. Experimental deburring results of target planning path and actual tool path of proximal side facet.

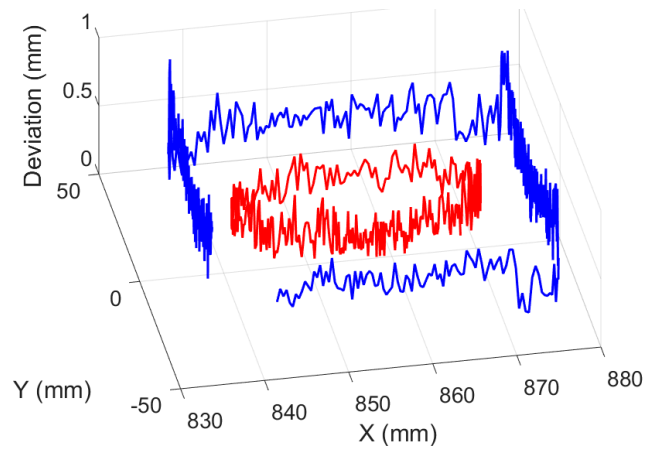


Figure 32. Deviation results of target planning path and actual tool path of experimental deburring for top facet.

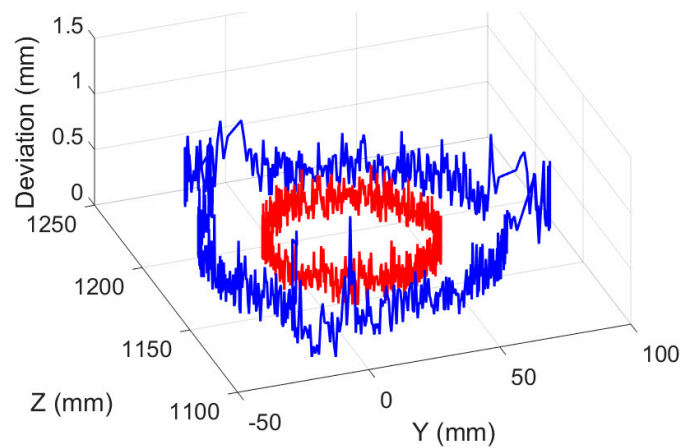


Figure 33. Deviation results of target planning path and actual tool path of experimental deburring for distal side facet.

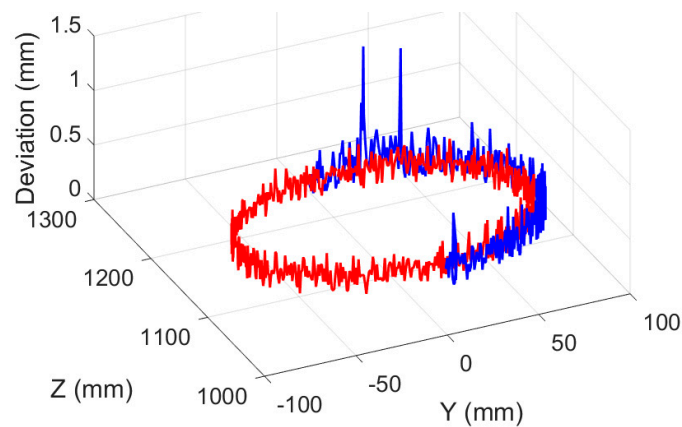


Figure 34. Deviation results of target planning path and actual tool path of experimental deburring for proximal side facet.

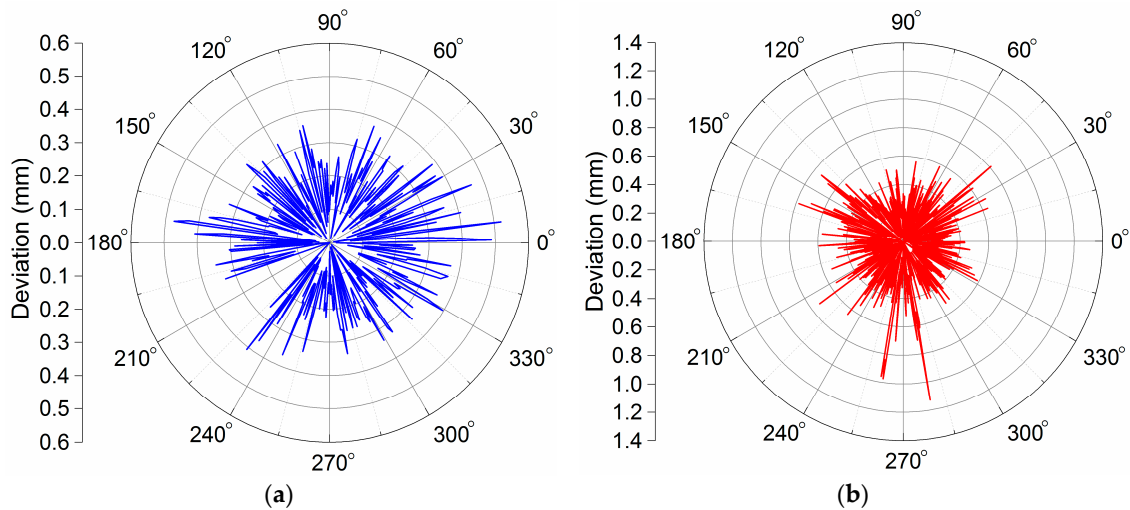


Figure 35. Deviation results of target planning path and actual tool path of experimental deburring for top facet (polar representation): (a) facet edges deburring deviation; (b) orifice edges deburring deviation.

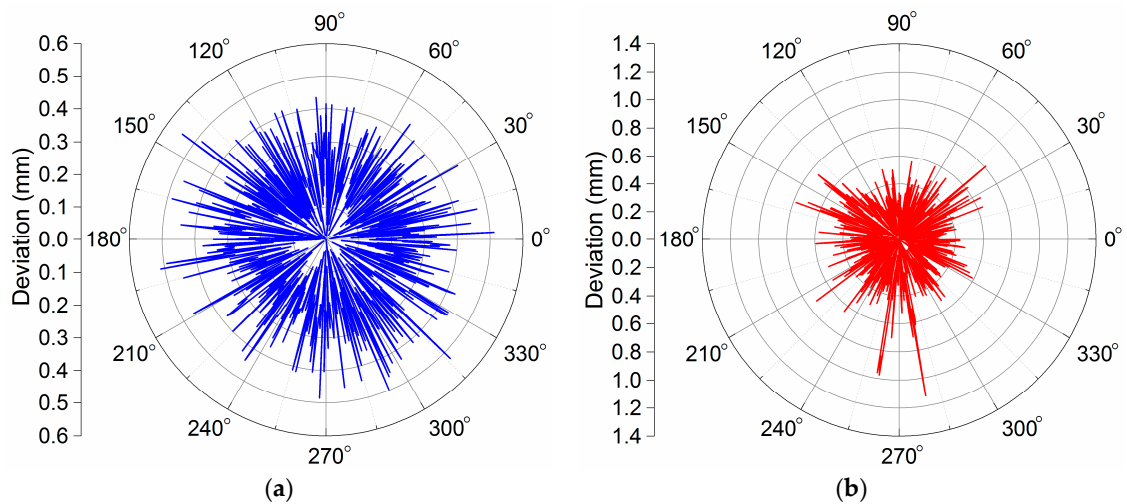


Figure 36. Deviation results of target planning path and actual tool path of experimental deburring for distal side facet (polar representation): (a) facet edges deburring deviation; (b) orifice edges deburring deviation.

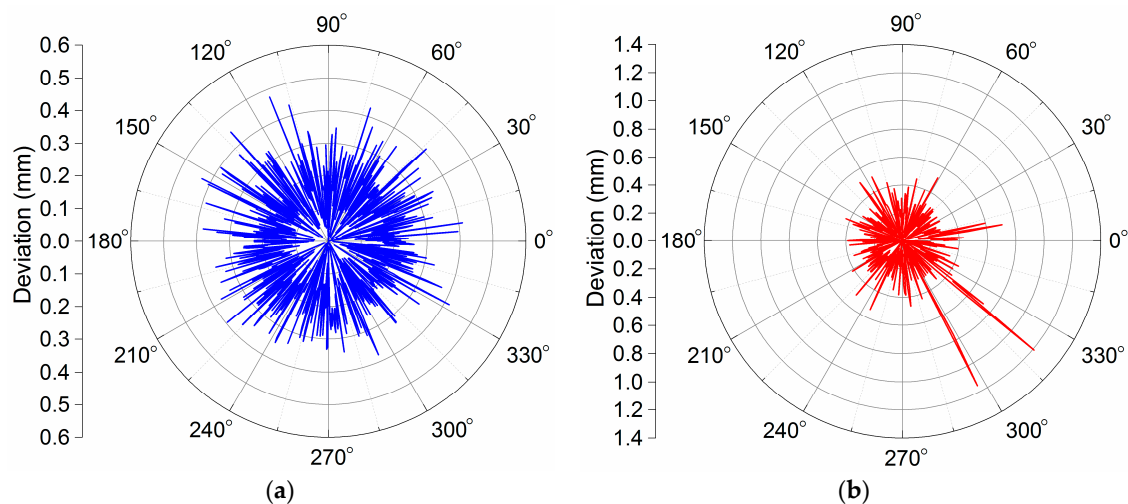


Figure 37. Deviation results of target planning path and actual tool path of experimental deburring for proximal side facet (polar representation): (a) facet edges deburring deviation; (b) orifice edges deburring deviation.

7. Conclusions

A new five-DOF hybrid robot manipulator and two experimental platforms were developed. For this robot manipulator, a new robotic deburring methodology for robotic deburring tool path planning and robotic deburring process parameter control was presented. The major contributions of this article can be summarized as follows:

1. The design structure and the physical structure of the robot manipulator for the original experimental platform and the improved one were developed, and the property characterizations of the dexterous manipulation reachability and the superior deburring capability in one setup were demonstrated. The robot manipulator can provide a good solution for the selection of the manufacturing equipment, such as deburring of the complex shaped parts.
2. A robotic deburring tool path planning method was proposed for the robotic deburring tool location (position and orientation) planning and the robotic layered deburring planning. Also, a robotic deburring process parameter control method based on fuzzy control for the robotic deburring was proposed, which represents the optimization property, convenience, simplicity, and implementation with automatic-online errors correction. These methods can be extended to handle similar problems for other types of the robot manipulators.
3. A dexterous manipulation experiment was conducted to verify the dexterous manipulation and the orientation reachability of the robot manipulator, especially the dexterous manipulation of a certain processing point. Furthermore, two robotic deburring experiments, i.e., a disc deburring experiment of an automobile hub and a multifaceted edges deburring experiment of an automobile steering booster housing, were conducted on the experimental platforms, and the effectiveness of the two proposed methods was verified, and the highly efficient and dexterous manipulation and deburring capacity of the robot manipulator for multifaceted deburring in one setup was also fully demonstrated.

In future work, several meaningful attempts need to be carried out, such as offline path correction, compensation for vibrations and/or chattering, backlash of ball screws and robot manipulator structural deformations, suppression for high frequency oscillations, and structural rigidity improvement of the robot manipulator. The two proposed methods are expected to provide some insight into the foundational aspects of robotic deburring tool path planning and robotic deburring process parameter control.

Author Contributions: All authors contributed to the research work and have read and approved the final manuscript.

Funding: This research was funded by Natural Science Basic Research Plan in Shaanxi Province of China (No. 2019JQ-426), Fundamental Research Funds for the Central Universities (No. 300102258107, 300102259308, 300102259401, 300102258402, 300102258305, 300103190365, 300102258205), Shaanxi Science and Technology Co-ordinated Innovation Project (No. 2016KTZDGY-02-03), Shaanxi International Science and Technology Cooperation Project (No. 2019KW-015) and Xi'an Science and Technology Project for Talented Personnel Service Enterprise in Colleges and Universities (No. 2017088CG/RC051(CADX001)).

Acknowledgments: Thanks to Mingrui Lv, Yafu Tian, Xiangjin Bu, Lianzheng Ge, Chongyang Wu, Chuqing Cao and Xunwei Tong for their help in the discussion and writing of the paper.

Conflicts of Interest: The authors declare no conflict of interest.

References

- Iglesias, I.; Ares, J.E.; Gonzalez-Gaya, C.; Morales, F.; Rosales, V.F. Predictive Methodology for Dimensional Path Precision in Robotic Machining Operations. *IEEE Access* **2018**, *6*, 49217–49223. [[CrossRef](#)]
- Roveda, L.; Pedrocchi, N.; Vicentini, F.; Tosatti, L.M. Industrial compliant robot bases in interaction tasks: A force tracking algorithm with coupled dynamics compensation Operations. *Robotica* **2017**, *35*, 1732–1746. [[CrossRef](#)]
- Robla-Gomez, S.; Becerra, V.M.; Llata, J.R.; Gonzalez-Sarabia, E.; Torre-Ferrero, C.; Perez-Oria, J. Working Together A Review on Safe Human-Robot Collaboration in Industrial Environments. *IEEE Access* **2017**, *5*, 26754–26773. [[CrossRef](#)]
- Stipanovic, T.; Jerbic, B.; Curkovic, P. A context-aware approach in realization of socially intelligent industrial robots. *IEEE Access* **2016**, *37*, 79–89. [[CrossRef](#)]
- Heydaryan, S.; Bedolla, J.S.; Belingardi, G. Safety Design and Development of a Human-Robot Collaboration Assembly Process in the Automotive Industry. *Appl. Sci.* **2018**, *8*, 344. [[CrossRef](#)]
- Ruppert, T.; Jasko, S.; Holczinger, T.; Abonyi, J. Enabling Technologies for Operator 4.0: A Survey. *Appl. Sci.* **2018**, *8*, 1650. [[CrossRef](#)]
- Chen, Y.; Dong, F. Robot machining: Recent development and future research issues. *Int. J. Adv. Manuf. Technol.* **2013**, *66*, 1489–1497. [[CrossRef](#)]
- Lai, C.Y.; Chavez, D.E.V.; Ding, S. Transformable parallel-serial manipulator for robotic machining. *Int. J. Adv. Manuf. Technol.* **2018**, *97*, 2987–2996. [[CrossRef](#)]
- Barnfather, J.D.; Abram, T. Efficient compensation of dimensional errors in robotic machining using imperfect point cloud part inspection data. *Measurement* **2018**, *117*, 176–185. [[CrossRef](#)]
- Mousavi, S.; Gagnol, V.; Bouzgarrou, B.C.; Ray, P. Dynamic modeling and stability prediction in robotic machining. *Int. J. Adv. Manuf. Technol.* **2017**, *88*, 3053–3065. [[CrossRef](#)]
- Barnfather, J.D.; Goodfellow, M.J.; Abram, T. A performance evaluation methodology for robotic machine tools used in large volume manufacturing. *Robot. Comput.-Integr. Manuf.* **2016**, *37*, 49–56. [[CrossRef](#)]
- Sabourin, L.; Subrin, K.; Cousturier, R.; Gogu, G.; Mezouar, Y. Redundancy-based optimization approach to optimize robotic cell behaviour: Application to robotic machining. *Ind. Robot Int. J.* **2015**, *42*, 167–178. [[CrossRef](#)]
- Caesarendra, W.; Pappachan, B.K.; Wijaya, T.; Lee, D.; Tjahjowidodo, T.; Then, D.; Manyar, O.M. An AWS Machine Learning-Based Indirect Monitoring Method for Deburring in Aerospace Industries Towards Industry 4.0. *Appl. Sci.* **2018**, *8*, 2165. [[CrossRef](#)]
- Pandiyani, V.; Caesarendra, W.; Tjahjowidodo, T.; Praveen, G. Predictive Modelling and Analysis of Process Parameters on Material Removal Characteristics in Abrasive Belt Grinding Process. *Appl. Sci.* **2017**, *7*, 363. [[CrossRef](#)]
- Xie, F.; Liu, X.-J.; Wang, C. Design of a novel 3-DoF parallel kinematic mechanism: Type synthesis and kinematic optimization. *Robotica* **2015**, *33*, 622–637. [[CrossRef](#)]
- Cheng, Y.-M.; Peng, W.-X.; Hsu, A.-C. Concentric hole drilling in multiple planes for experimental investigation of five-axis reconfigurable precision hybrid machine. *Int. J. Adv. Manuf. Technol.* **2015**, *76*, 1253–1262.
- Sangveraphunsiri, V.; Chooprasird, K. Dynamics and control of a 5-DOF manipulator based on an H-4 parallel mechanism. *Int. J. Adv. Manuf. Technol.* **2011**, *52*, 343–364. [[CrossRef](#)]

18. Altuzarra, O.; Martín, Y.S.; Amezua, E.; Hernández, A. Motion pattern analysis of parallel kinematic machines: A case study. *Robot. Comput.-Integr. Manuf.* **2009**, *25*, 432–440. [[CrossRef](#)]
19. Wang, L.; Wu, J.; Li, T.; Wang, J.; Gao, G. A study on the dynamic characteristics of the 2-dof redundant parallel manipulator of a hybrid machine tool. *Int. J. Robot. Autom.* **2015**, *30*, 184–191. [[CrossRef](#)]
20. Wang, L.; Wu, J.; Wang, J.; You, Z. An experimental study of a redundantly actuated parallel manipulator for a 5-DOF hybrid machine tool. *IEEE/ASME Trans. Mech.* **2009**, *14*, 72–81. [[CrossRef](#)]
21. Li, Q.; Wu, W.; Li, H.; Wu, C. A hybrid robot for friction stir welding. *Proc. Inst. Mech. Eng. Part C J. Mech. Eng. Sci.* **2015**, *229*, 2639–2650. [[CrossRef](#)]
22. Zoppi, M.; Zlatanov, D.; Molfino, R. Kinematics analysis of the Exechon tripod. In Proceedings of the ASME 2010 International Design Engineering Technical Conferences and Computers and Information in Engineering Conference, Montreal, QC, Canada, 15–18 August 2010; pp. 1381–1388.
23. Niknam, S.A.; Davoodi, B.; Paulo Davim, J.; Songmene, V. Mechanical deburring and edge-finishing processes for aluminum parts—A review. *Int. J. Adv. Manuf. Technol.* **2018**, *95*, 1101–1125. [[CrossRef](#)]
24. Niknam, S.A.; Songmene, V. Milling burr formation, modeling and control: A review. *Proc. Inst. Mech. Eng. Part B J. Eng. Manuf.* **2015**, *229*, 893–909. [[CrossRef](#)]
25. Burghardt, A.; Szybicki, D.; Kurc, K.; Muszynska, M.; Mucha, J. Experimental Study of Inconel 718 Surface Treatment by Edge Robotic Deburring with Force Control. *Strength Mater.* **2017**, *49*, 594–604. [[CrossRef](#)]
26. Villagrossi, E.; Cenati, C.; Pedrocchi, N.; Beschi, M.; Tosatti, L.M. Flexible robot-based cast iron deburring cell for small batch production using single-point laser sensor. *Int. J. Adv. Manuf. Technol.* **2017**, *92*, 1425–1438. [[CrossRef](#)]
27. Kosler, H.; Pavlovčič, U.; Jezeršek, M.; Možina, J. Adaptive Robotic Deburring of Die-Cast Parts with Position and Orientation Measurements Using a 3D Laser-Triangulation Sensor. *Strojniški Vestnik-J. Mech. Eng.* **2016**, *62*, 207–212. [[CrossRef](#)]
28. Caggiano, A.; Marzano, A.; Teti, R. Sustainability Enhancement of a Turbine Vane Manufacturing Cell through Digital Simulation-Based Design. *Energies* **2016**, *9*, 790. [[CrossRef](#)]
29. Song, H.-C.; Song, J.-B. Precision robotic deburring based on force control for arbitrarily shaped workpiece using CAD model matching. *Int. J. Precis. Eng. Manuf.* **2013**, *14*, 85–91. [[CrossRef](#)]
30. Villagrossi, E.; Pedrocchi, N.; Beschi, M.; Tosatti, L.M. A human mimicking control strategy for robotic deburring of hard materials. *Int. J. Comput. Integr. Manuf.* **2018**, *31*, 869–880. [[CrossRef](#)]
31. Gracia, L.; Ernesto Solanes, J.; Munoz-Benavent, P.; Miro, J.V.; Perez-Vidal, C.; Tornero, J. Adaptive Sliding Mode Control for Robotic Surface Treatment Using Force Feedback. *Measurement* **2018**, *52*, 102–118. [[CrossRef](#)]
32. Ernesto Solanes, J.; Gracia, L.; Munoz-Benavent, P.; Esparza, A.; Miro, J.V.; Tornero, J. Adaptive robust control and admittance control for contact-driven robotic surface conditioning. *Robot. Comput.-Integr. Manuf.* **2018**, *54*, 115–132. [[CrossRef](#)]
33. Pillai, J.U.; Sanghrajka, I.; Shunmugavel, M.; Muthuramalingam, T.; Goldberg, M.; Littlefair, G. Optimisation of multiple response characteristics on end milling of aluminium alloy using Taguchi-Grey relational approach. *Measurement* **2018**, *124*, 291–298. [[CrossRef](#)]
34. Tao, Y.; Zheng, J.; Lin, Y. A Sliding Mode Control-based on a RBF Neural Network for Deburring Industry Robotic Systems. *Int. J. Adv. Robot. Syst.* **2016**, *13*, 1–10. [[CrossRef](#)]
35. Tao, Y.; Zheng, J.; Lin, Y.; Wang, T.; Xiong, H.; He, G.; Xu, D. Fuzzy PID control method of deburring industrial robots. *J. Intell. Fuzzy Syst.* **2015**, *29*, 2447–2455. [[CrossRef](#)]
36. Chen, C.-Y.; Shieh, S.-S.; Cheng, M.-Y.; Su, K.-H. Vision-based Pythagorean hodograph spline command generation and adaptive disturbance compensation for planar contour tracking. *Int. J. Adv. Manuf. Technol.* **2013**, *65*, 1185–1199. [[CrossRef](#)]
37. Aggogeri, F.; Borboni, A.; Faglia, R.; Merlo, A.; Pellegrini, N. A kinematic model to compensate the structural deformations in machine tools using fiber Bragg grating (FBG) sensors. *Appl. Sci.* **2017**, *7*, 114. [[CrossRef](#)]
38. Borboni, A.; Faglia, R. *Parasitic Phenomena in the Dynamics of Industrial Devices*; CRC Press: Boca Raton, FL, USA, 2011.
39. Aggogeri, F.; Borboni, A.; Merlo, A.; Pellegrini, N.; Ricatto, R. Vibration Damping Analysis of Lightweight Structures in Machine Tools. *Materials* **2017**, *10*, 297. [[CrossRef](#)]
40. Wang, M.; Zan, T.; Gao, X.; Li, S. Suppression of the time-varying vibration of ball screws induced from the continuous movement of the nut using multiple tuned mass dampers. *Int. J. Mach. Tools Manuf.* **2016**, *107*, 41–49. [[CrossRef](#)]

41. Guo, W.; Li, R.; Cao, C.; Gao, Y. Kinematics, dynamics, and control system of a new 5-degree-of-freedom hybrid robot manipulator. *Adv. Mech. Eng.* **2016**, *8*, 1687814016680309. [[CrossRef](#)]
42. Guo, W.; Li, R.; Cao, C.; Gao, Y. Kinematics Analysis of a Novel 5-DOF Hybrid Manipulator. *Int. J. Autom. Technol.* **2015**, *9*, 765–774. [[CrossRef](#)]
43. Guo, W.; Li, R.; Cao, C.; Gao, Y. A Novel Method of Dexterity Analysis for a 5-DOF Manipulator. *J. Robot.* **2016**, *2016*, 8901820. [[CrossRef](#)]
44. Guo, W.; Li, R.; Cao, C.; Tong, X.; Gao, Y. A New Methodology for Solving Trajectory Planning and Dynamic Load-Carrying Capacity of a Robot Manipulator. *Math. Prob. Eng.* **2016**, *2016*, 1302537. [[CrossRef](#)]
45. Kalpakjian, S.; Schmid, S.R. *Manufacturing Engineering and Technology*; Prentice Hall: Upper Saddle River, NJ, USA, 2000.
46. Albertelli, P.; Keshari, A.; Matta, A. Energy oriented multi cutting parameter optimization in face milling. *J. Clean. Prod.* **2016**, *137*, 1602–1618. [[CrossRef](#)]
47. Das, S.R.; Dhupal, D.; Kumar, A. Experimental investigation into machinability of hardened AISI 4140 steel using TiN coated ceramic tool. *Measurement* **2015**, *62*, 108–126. [[CrossRef](#)]
48. Maher, I.; Eltaib, M.E.H.; Sarhan, A.A.D.; El-Zahry, R.M. Investigation of the effect of machining parameters on the surface quality of machined brass (60/40) in CNC end milling-ANFIS modeling. *Int. J. Adv. Manuf. Technol.* **2014**, *74*, 531–537. [[CrossRef](#)]
49. Ko, P.-J.; Tsai, M.-C. H-infinity Control Design of PID-Like Controller for Speed Drive Systems. *IEEE Access* **2018**, *6*, 36711–36722. [[CrossRef](#)]
50. Szczecinski, N.S.; Hunt, A.J.; Quinn, R.D. Design process and tools for dynamic neuromechanical models and robot controllers. *Biol. Cybern.* **2017**, *111*, 105–127. [[CrossRef](#)]
51. Amezcua-Brooks, L.; Liceaga-Castro, J.; Liceaga-Castro, E. Speed and Position Controllers Using Indirect Field-Oriented Control: A Classical Control Approach. *IEEE Trans. Ind. Electron.* **2014**, *61*, 1928–1943. [[CrossRef](#)]
52. Ajwad, S.A.; Iqbal, J.; Ul Islam, R.; Alsheikhy, A.; Almeshal, A.; Mehmood, A. Optimal and Robust Control of Multi DOF Robotic Manipulator: Design and Hardware Realization. *Cybern. Syst.* **2018**, *49*, 77–93. [[CrossRef](#)]
53. Reiner, M.J.; Zimmer, D. Object-oriented modelling of wind turbines and its application for control design based on nonlinear dynamic inversion. *Math. Comput. Model. Dyn. Syst.* **2017**, *23*, 319–340. [[CrossRef](#)]
54. Prieto-Araujo, E.; Egea-Alvarez, A.; Fekriasl, S.; Gomis-Bellmunt, O. Multi-Shaker Control A Review of the Evolving State-of-the-Art. *IEEE Trans. Power Deliv.* **2016**, *31*, 575–585. [[CrossRef](#)]
55. Al-Darraj, I.; Kilic, A.; Kapucu, S. Mechatronic design and genetic-algorithm-based MIMO fuzzy control of adjustable-stiffness tendon-driven robot finger. *Mech. Sci.* **2018**, *9*, 277–296. [[CrossRef](#)]
56. Chen, Z.; Li, Z.; Chen, C.L.P. Disturbance Observer-Based Fuzzy Control of Uncertain MIMO Mechanical Systems with Input Nonlinearities and its Application to Robotic Exoskeleton. *IEEE Trans. Cybern.* **2017**, *47*, 984–994. [[CrossRef](#)]
57. Wang, W.-Y.; Chien, Y.-H.; Leu, Y.-G.; Hsu, C.-C. Mean-Based Fuzzy Control for a Class of MIMO Robotic Systems. *IEEE Trans. Fuzzy Syst.* **2016**, *24*, 966–980. [[CrossRef](#)]
58. Mendes, N.; Neto, P. Indirect adaptive fuzzy control for industrial robots: A solution for contact applications. *Expert Syst. Appl.* **2015**, *42*, 8929–8935. [[CrossRef](#)]

